Backward erosion piping in numerical models

A literature review

van der Linde, E. M.; Wewer, M.; Robbins, B. A.; Colomés, O.; Jonkman, S. N.; Aguilar-López, J. P.

DOI
10.1016/j.envsoft.2025.106681

Publication date
2025

Document Version
Final published version

Published in
Environmental Modelling and Software

Citation (APA)
van der Linde, E. M., Wewer, M., Robbins, B. A., Colomés, O., Jonkman, S. N., & Aguilar-López, J. P. (2025). Backward erosion piping in numerical models: A literature review. *Environmental Modelling and Software*, *194*, Article 106681. https://doi.org/10.1016/j.envsoft.2025.106681

Environmental Modelling and Software 194 (2025) 106681

Contents lists available at ScienceDirect

Environmental Modelling and Software

journal homepage: www.elsevier.com/locate/envsoft

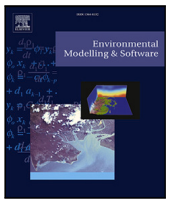

Backward erosion piping in numerical models: A literature review

E.M. van der Linde [a,b,*], M. Wewer [c], B.A. Robbins [d], O. Colomés [a], S.N. Jonkman [a], J.P. Aguilar-López [a]

[a] Hydraulic Engineering Department Delft University of Technology, Stevinweg 1, Delft, 2628 CN, Zuid Holland, The Netherlands
[b] Flood Defence Technology Deltares, Boussinesqweg 1, Delft, 2629 HV, Zuid Holland, The Netherlands
[c] Dresden University of Technology, August-Bebel-Straße 30, Dresden, 01219, Sachsen, Germany
[d] U.S. Army Corps of Engineers, 12596 W Bayaud Avenue, Lakewood, Suite 400, CO, United States of America

ARTICLE INFO

Keywords:
Backward erosion piping
Numerical modelling
Internal erosion
Dams
Levees

ABSTRACT

Backward erosion piping is a failure mechanism of dikes. Numerical modelling is crucial for design and assessment against BEP. Over 30 models have been developed, each with a different purpose and approach. This paper provides a comprehensive overview of the available numerical BEP models, highlighting their limitations, capabilities, and associated challenges. It discusses the different assumptions and their implications on the representation of BEP. Key challenges in the numerical modelling of BEP are (1) the flow (regime) inside the pipe, which is often simplified, even though the impact of this is relatively unknown. (2) The type of erosion (primary or secondary) differs per model, and even within a given type of erosion, approaches vary. (3) Overcoming the difference in scale is a trade-off between the computational effort and simplification. (4) Furthermore, validation of the physics in BEP modelling is difficult due to a of lack micro-scale experimental data.

Contents

* Corresponding author at: Hydraulic Engineering Department Delft University of Technology, Stevinweg 1, Delft, 2628 CN, Zuid Holland, The Netherlands.
E-mail address: e.m.vanderlinde@tudelft.nl (E.M. van der Linde).

https://doi.org/10.1016/j.envsoft.2025.106681
Received 14 April 2025; Received in revised form 28 August 2025; Accepted 3 September 2025
Available online 11 September 2025

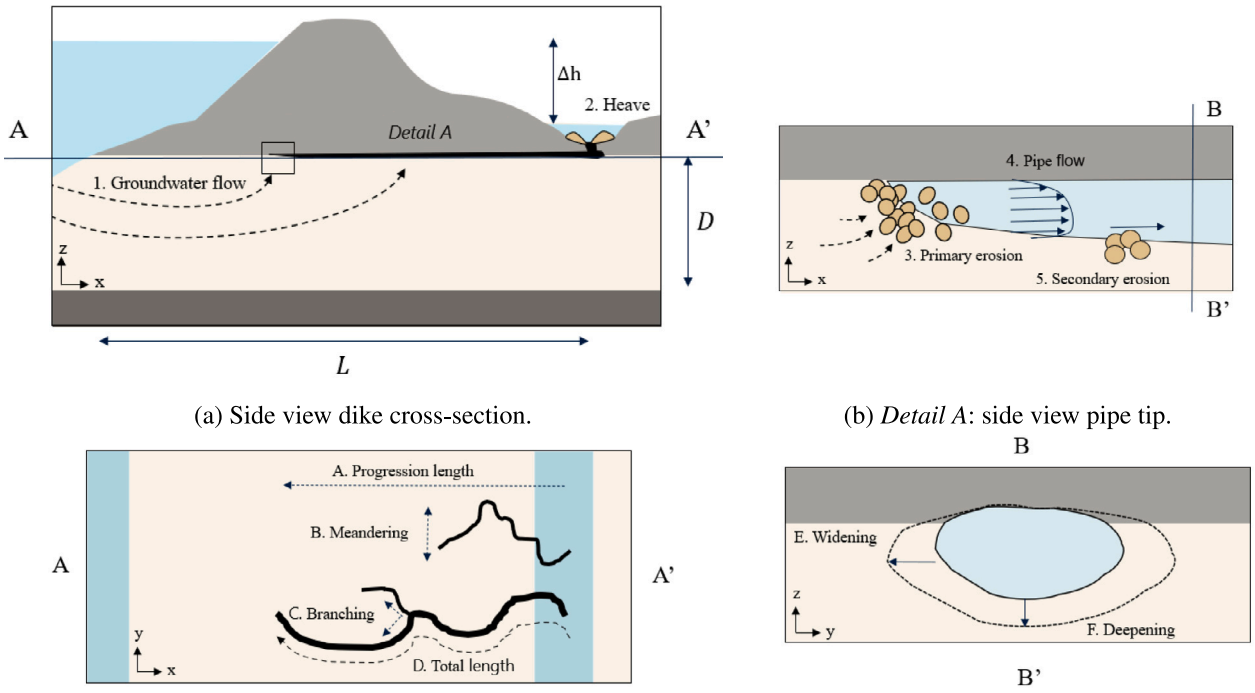

(a) Side view dike cross-section.

(b) *Detail A*: side view pipe tip.

(c) Top view dike at A-A'.

(d) *Detail A*: Front view pipe at B-B'.

Fig. 1. Backward Erosion piping is governed by the physics shown in (a) and (b). Groundwater flow towards the pipe and outlet (1) leads to the heave at the outlet (2) if no pipe is present or the removal of sediments at the pipe tip if a pipe has started to form (3). The flow inside the pipe (4) leads to the removal of sediments from the bottom and walls of the pipe (5). The morphology of the pipe is shown in (c) and (d). The progression length is the distance (from downstream to upstream) the pipe has grown (A). The pipe meanders through the soil (B) if the pipe splits up and/or merges again, this is called branching (C). The total length of the pipe is the length along the entire pipe path (D) and due to secondary erosion, the pipe widens (E) and deepens (F).

1. Introduction

Backward erosion piping (BEP) is a failure mechanism of water retaining structures, which has accounted for approximately 15% of historic dike and dam failures (Danka and Zhang, 2015; Foster et al., 2000). During high water events, the hydraulic head (h [m]) increases on the upstream side, the subsequent groundwater flow can cause sand grains to erode from the foundation leading to the formation of one or more erosion channels, commonly referred to as "pipes" (Fig. 1). In case the top layer is cohesive and non-permeable, it is referred to as the blanket layer. Piping can only occur if there is an opening in the blanket layer. This opening can be anthropogenic, for instance due to the excavation of a ditch or it can be created during the high water event when uplift causes the tearing of the blanket layer. When such an opening through the blanket layer is present, heave (the fluidization of sand) must occur at the bottom of the blanket layer for BEP to initiate.

During the progression of BEP, groundwater flow towards the pipe leads to the removal of sediments at the pipe tip. This process is referred to as primary erosion and results in the lengthening of the pipe. The flow inside the pipe leads to the removal of sediments from the bottom and walls of the pipe; this is called secondary erosion (Hanses, 1985). These erosion processes (combined with deposition processes) lead to the lengthening, widening, deepening, meandering, and branching of the pipe. The process and terminology of BEP are described in Fig. 1.

In the design and assessment of water retaining structures, a common proxy to determine if BEP can occur is the critical head gradient, which has been used since the early 20th century. This is calculated by dividing the critical head difference (Δh_c [m]) by the seepage length (L [m]). By studying weirs in India, Bligh and Griffith (Bligh, 1910; Griffith, 1914) developed the first BEP assessment models. In these models, the critical head gradient is related to a material-dependent creep factor. The seepage length in these formulations is the path along which the pipe is expected to grow. Lane (1935) discovered that the vertical seepage length contributes three times more to the safety of the structure than the horizontal seepage length and he adjusted the model accordingly. Initiated by flood events in the mid-twentieth century, further research was performed in the Netherlands, Germany and the United States to better define BEP (Robbins, 2022). This led to a better understanding of the failure mechanism and improved semi-analytical models which relate measurable parameters of the subsoil and aquifer to BEP. In the late 1980s Sellmeijer developed a semi-analytical design rule based on groundwater flow in the aquifer and laminar flow inside the pipe as well as a grain equilibrium condition for erosion. Because of this theoretical derivation, the design rule includes measurable soil parameters such as the permeability (κ [m^2]) and grain-size (d_{70} [m]) as well as the aquifer depth (D [m], see Fig. 1). Experimental and numerical studies were used to calibrate and fine-tune this design rule (Sellmeijer et al., 1989; Sellmeijer and Koenders, 1991; Sellmeijer et al., 2011). Schmertmann (2000) developed a different method based on a data set of 115 BEP lab-experiments. He defined a set of factors that influence BEP and proposed corresponding scaling factors between lab experiments and field situations. These factors include, among others, the anisotropy of the hydraulic conductivity, the uniformity coefficient and layers in the aquifer. Another approach was developed by Ojha et al. (2003), whose model assumes groundwater flow can be idealized as flow through a network of parallel pipes with diameters equal to the mean grain size. The models by Schmertmann (2000) and Ojha et al. (2003) do not include the influence of the pipe on the groundwater flow. Hoffmans and Rijn (2018) proposed an alternative approach, which simplifies the groundwater flow and uses a Shields' based erosion criterion for erosion. Within the past decade, research has focused on expanding the current knowledge of the erosion process, groundwater flow and pipe flow as well as the effectiveness of different countermeasures such as cut-off walls which act as impermeable barriers and filters such as the coarse sand barrier (Rosenbrand and Van Beek, 2021). Because of this, more information is now available on the

3D nature of BEP (Vandenboer et al., 2014; Van Beek et al., 2022), pipe dimensions (Vandenboer et al., 2019) and primary erosion (Robbins and Griffiths, 2022; Xiao et al., 2019). More comprehensive historical overviews of BEP experiments and analytical/empirical models are available (Van Beek et al., 2011; Vandenboer, 2019; Allan, 2018; Rice et al., 2021; Robbins, 2022).

The previously mentioned analytical/empirical models are all based on (relatively) homogeneous soils and 2D geometries or experimental set-ups. Numerical models have been developed since the beginning of the 21st century to model the more complex reality; however, there is not yet a model that can incorporate all fundamental aspects of backward erosion piping for the design and assessment of dikes. This paper aims to give a state-of-the-art overview of the different numerical BEP models, their capabilities, and main limitations. In addition, this paper aims to address and discuss some of the main challenges of the numerical modelling of BEP. To limit the scope of the research, all analysed papers satisfy two criteria:

1. All papers use numerical methods to solve the governing equations.
2. The models include a hollow pipe zone in the foundation, This can be either predefined or develop during the simulation.

Therefore, this review excludes methods that only consider heave. In the literature the term 'piping' is sometimes used to describe other internal erosion mechanisms. The International Commission on Large Dams (ICOLD) defined BEP as one of four internal erosion mechanisms, the others being suffusion, concentrated leak erosion, and contact erosion (ICOLD, 2017) (see Fig. 2). According to Robbins and Griffiths (2018a), concentrated leak erosion (CLE) refers to any process in which water flows freely through an open space, eroding the soil along the boundary of the opening. Although by this definition CLE is not bound by soil type, during CLE the defects must be able to sustain themselves without collapsing which is more likely in cohesive soils. The defects can be caused by anthropogenic influences, tensile cracking or hydraulic fractures (Bonelli, 2013). CLE is similar to secondary erosion in BEP as was pointed out by Bonelli (2013). When a fine granular material is in contact with a coarse granular material, contact erosion can occur. This is the process where grains from the fine layer are transported through the pores of the coarse layer, thus forming a hollow space. Suffusion can occur when there is a widely graded or gap-graded soil, finer particles from the soil matrix are eroded while the coarser skeleton remains (Bonelli, 2013). The remaining skeleton is more porous/permeable than the original soil with fines. When suffusion is accompanied by volume loss, it is referred to as suffosion (Fannin and Slangen, 2014). A possible combination of these internal erosion mechanisms with BEP is the assumption that suffusion occurs in front of the pipe tip.

Numerical models that mention BEP but use methods that better describe other internal erosion mechanisms are not included in this review, unless a new modelling approach was used that is transferable to BEP modelling.

Published research on the numerical modelling of BEP has mainly focused on the physical representation of the process. Only a few studies address computational aspects such as mesh convergence, regularization issues, stability, accuracy of the methods, and potential solver choices. Because of the limited research, these computational aspects are not included in the current paper.

In total 37 unique numerical models for BEP have been identified and analysed. Multiple papers by the same authors that describe the same numerical model are excluded. The included papers are shown in Table 1.

Earlier literature studies have classified BEP models based on the governing equations, the representation of the pipe and its progression (Wang et al., 2014; Robbins, 2022). However, combined methods such as machine learning models and multi-physics models cannot be captured in this classification. This paper does not aim to reclassify these papers. Instead, different model components are described, compared, and criticized with a focus on identifying knowledge gaps.

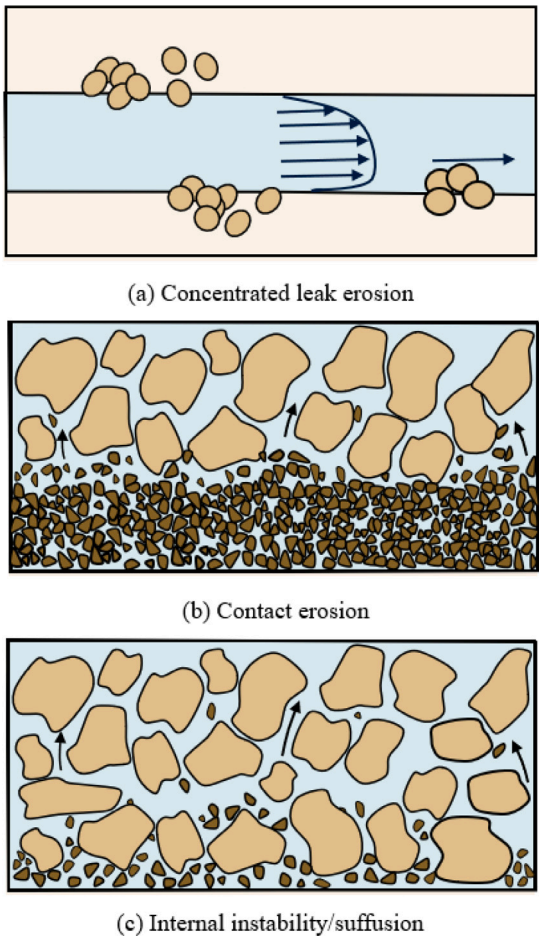

Fig. 2. Internal erosion mechanisms (excluding BEP).

In the next chapter, the spatial and temporal scales of BEP modelling are described. Groundwater flow, computational fluid dynamics, and pipe flow equations are discussed in Section 3. The modelling approaches for primary and secondary erosion are discussed in Section 4. The paper ends with a general discussion and concluding remarks.

2. Scale

Numerical BEP models operate at different scales. Both the spatial scales – relating to the size and dimensions of the model – and temporal scales are discussed below.

2.1. Spatial scale

In this paper, two different process scales are distinguished, the micro- and macro-scale. The micro-scale in BEP modelling refers to the grain-level erosion processes (Fig. 3). The macro-scale refers to the full process of pipe development from downstream to upstream.

In addition to the process scales, an experimental scale is also distinguished, because validation of the numerical modelling is done using physical experiments with different seepage lengths. Small-scale experiments refer to experiments with seepage lengths less than 1 m. Medium-scale experiments have seepage lengths between 1 and 6 m. Large-scale experiments have seepage lengths of more than 6 m. At the field scale (real dikes), seepage lengths may exceed 100 m. As

Table 1
Numerical BEP models sorted by date. Other overviews of BEP numerical modelling papers can be found in the works of Allan (2018) and Robbins (2022).

Reference	Scale		Flow		Erosion	Validation/Calibration	Numerical	
Citation	Spatial	Temporal[a]	Aquifer	Pipe	Type[b]	Experiments	Software[e]	Method[f]
Sellmeijer (2006)	2D	QSS	Darcy	Linear equation	S	0	MSeep	FEM
Ding et al. (2007)	3D	QSS	Darcy	Linear equation	P	0	Unknown	FEM
Shamy and Aydin (2008)	3D	TD	NS	NS	N	0	PFC^{3D}	DEM
Zhou et al. (2012)	2D	QSS	Darcy	Linear equation	S	2 small-scale	Unknown	EFG
Bersan et al. (2013)	2D/3D	SS	BF	Stokes	–	1 small-scale	Comsol	FEM
Kanning and Calle (2013)	2D top	QSS	Darcy	K-Amplification	P	0	Custom	FDM
Esch et al. (2013)	2D	QSS	Darcy	Linear equation	S	0	DgFlow	FEM
Wang and Ni (2013)	3D	TD	NS	NS	N	6 small-scale	PFC^{3D}	DEM
Vandenboer et al. (2014)	3D	SS	Darcy	K-Amplification	–	1 small-scale	Abaqus	FEM
Wang et al. (2014)	2D	QSS	Darcy	Linear equation	PT	2 small-scale	Unkown	EFG
Aguilar-López et al. (2016)	2D	SS	Darcy	Linear equation	S	0	Comsol	FEM
Fujisawa (2016)	2D top	TD	BF	NS	PT	0	Custom	FVM
Robbins (2016)	3D	QSS	Darcy	K-Amplification	P	1 medium-scale 1 small-scale	FLAC3D	FDM
Navin and Shewbridge (2017)	2D	SS	Darcy	K-Amplification	–	0	SEEP/W	FEM
Rotunno et al. (2017)	2D	TD	Darcy	Linear equation	PST	1 large-scale	FEAP	FEM
Tran et al. (2017)	2D	TD	LBM	LBM	N	0	Custom	DEM
Robbins and Griffiths (2018b)	2D/3D	QSS	Darcy	Linear equation	PS	0	S& G FEM	FEM
Fascetti and Oskay (2019a)	3D	QSS	Darcy	K-Amplification	P	1 medium-scale 4 small-scale	Custom	FVM
Fascetti and Oskay (2019b)[c]	2D	TD	Darcy	K-Amplification	I	4 large-scale	Custom	FVM
Froiio et al. (2019)	2D	TD	LBM	LBM	N	0	Custom	DEM
Rotunno et al. (2019)	2D/3D	TD	Darcy	Linear equation	PST	4 large-scale	FEAP	FEM
Saliba et al. (2019)	2D	QSS	Darcy	K-Amplification	P	0	PLAXIS	FEM
Barendsen (2020)	2D/3D	SS	Darcy	K-Amplification	–	3 large-scale	iMOD/MSeep	FEM/FEM
Callari and Froiio (2020)[c]	2D/3D	TD	Darcy	Linear equation	PST	7 non-BEP[d]	FEAP	FEM
Rahimi and Shafieezadeh (2020)	3D	QSS	Darcy	K-Amplification	P	1 small-scale	FLAC3D	FDM
Rahimi et al. (2021)	3D	QSS	Darcy	K-Amplification	P	3 small-scale	FLAC3D	FDM
Robbins and Griffiths (2021a)	2D top	QSS	Darcy	Linear equation	PS	0	Custom	FEM
Robbins et al. (2021)	2D top	QSS	Darcy	Linear equation	PS	0	Custom	FEM
Wewer et al. (2021)	2D	TD	Darcy	Linear equation	ST	3 large-scale	Comsol	FEM
Nie et al. (2022)	3D	TD	NS	NS	N	0		DEM
Robbins (2022)	3D	QSS	Darcy	Linear equation	PS	3 medium-scale 2 small-scale	Custom	FEM
Van Beek et al. (2022)	3D	QSS	Darcy	Linear equation	S	5 large-scale 6 medium-scale 14 small-scale	DgFlow	FEM
Xiao et al. (2023)	3D	SS	Darcy	Linear equation	–	1 small-scale	Abaqus	FEM
Pol et al. (2024)	3D	TD	Darcy	Linear equation	ST	1 large-scale 6 small-scale	DgFlow	FEM
Ma et al. (2024)[c]	2D	TD	Darcy	K-Amplification	I	0	Custom	SPH
Okamura and Kusube (2025)	3D	QSS	Darcy	Linear equation	S	7 centrifuge	Unknown	Unknown

[a] SS: steady-state, QSS: quasi-steady-state, TD: time-dependent.

[b] P: primary erosion, S: secondary erosion, N: Newton's second law of motion, T: transport equations, I: internal erosion, -: no erosion.

[c] Although the imposed erosion criteria or applications of these models are not BEP, they are included in this table, because of notable methods or conceptualizations that are also applicable in BEP modelling.

[d] Validation is found in a different paper or report.

[e] Software used, Custom refers to a custom-made or in-house code. S& G FEM refers to the Finite Element Software by Smith and Griffiths (2004).

[f] FEM: Finite Element Method, FDM: Finite Difference Method, FVM: Finite Volume Method, DEM: Discrete Element Method, EFG: Element Free Galerkin, SPH: Smooth Particle Hydrodynamics.

shown in Table 1, there are not many medium-scale and large-scale experiments used in the validation/calibration of the numerical models, due to limited availability. However, the medium-scale and large-scale experiments that are available have limited micro-scale measurements, thus making it difficult to validate micro-scale processes at larger scales.

Micro-scale erosion processes can be modelled using the discrete element method (DEM), in which each grain is modelled separately. The grains move according to Newton's second law of motion ($\Sigma F = ma$), which states that if there is a residual force acting on a given mass, the mass (grain) accelerates. The main driving force (F [N]) acting on soil grains in BEP is the drag force caused by flow of water. This force is calculated using either the incompressible Navier–Stokes (NS) equations or the Lattice Boltzmann method (LBM) (see Section 3.2). DEM was first introduced in BEP modelling by Shamy and Aydin (2008). They modelled BEP in a 3D small-scale set-up ($L = 0.05$ m). The commercial software package PFC^{3D} was used to couple NS with DEM. The grain diameters ranged from $1.7E^{-3}$ to $8.5E^{-3}$ m, therefore only roughly 10 grains exist in the seepage length. However, in field scale situations seepage lengths can be larger than 100 m and the grains may be as small as $1.0E^{-3}$ m. The authors noted that the influence of up-scaling these particles was a major limitation of the approach (Shamy and Aydin, 2008).

To overcome scaling issues, similarity criteria (scaling laws) between DEM and experiments were derived (Wang and Ni, 2013; Ni et al., 2015). These similarity criteria were derived from groundwater flow equations; however, no erosion component was considered in the scaling. Therefore, the proposed similarity criteria require more validation for the erosion processes. Primary erosion (Fig. 1) has been studied using the LBM-DEM method (Tran et al., 2017; Froiio et al., 2019). Erosion due to tangential flow (although not in BEP modelling) has also been modelled using LBM-DEM, for example by modelling a

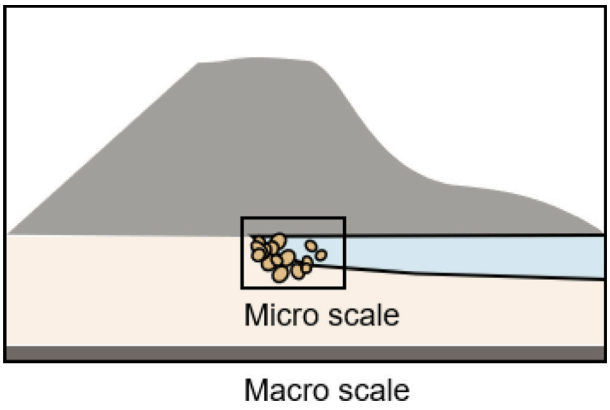

Fig. 3. The pipe tip is considered the micro-scale. Because the pipe progresses over the entire length over the dike, this is considered the macro-scale. When considering an entire flood defence system, often with many cross sections, the system scale is considered.

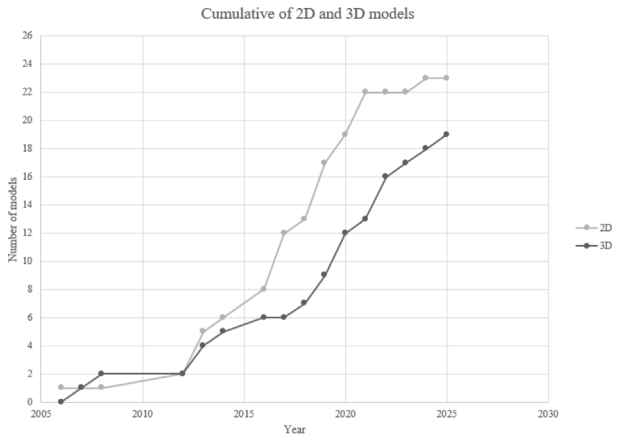

Fig. 4. The development of 2D and 3D models between 2006–2025. The papers used for this graph are shown in Table 1.

hole erosion test (Lominé et al., 2013; Sibille et al., 2015). The DEM studies mentioned above demonstrate the suitability of DEM modelling to learn more about small-scale BEP processes. However, as the erosion and the flow between the pores happen at the micro-scale, small mesh elements and small time steps are required in the computations. Because of this, DEM modelling is computationally expensive. One study reported computation times of 30 days in a 2D calculation of a small-scale problem (L = 0.24 m) (Froiio et al., 2019), therefore it is not suitable for engineering practice.

With the improvements of efficiency and increased numerical capacity, the application in BEP modelling is expected to increase. However, in the near future, DEM will mainly be used for research to better understand the micro-scale erosion process. In the long term, DEM could be coupled with continuum models to provide a BEP model for engineering practice that adequately captures both the macro-scale and micro-scale aspects of the process.

At the macro-scale, continuum partial differential equation solution methods such as Finite Difference/Volume Methods (FDM/FVM) (7 models), Finite Element Methods (FEM) (21 models) or the mesh-free method Element Free Galerkin (EFG) (2 models) are applied. In these methods, the aquifer and pipe are modelled as one continuum (one set of governing equations) or two continua (two sets of governing equations with a boundary condition on the interface) (Fujisawa and Murakami, 2018). Because continuum models cannot represent the micro-scale erosion phenomena, empirical equations for determining the grain stability are combined with the numerical models to represent the erosion. The computational effort of these models is highly dependent on the discretization and dimensions of the domain. In particular, the representation of the pipe and the overall model dimensions significantly impact computational effort, as they determine the number of mesh elements required. For example, the pipe in BEP is either represented as a multi-dimensional (2D/3D) space or as a one-dimensional domain. If the pipe has physical dimensions, a large number of elements is required to represent this zone and the zone around it. An advantage of this approach is that the flow can be fully resolved using the Navier–Stokes equations. In the aquifer, larger mesh elements can be applied. However, because the elements in the pipe are very small and the element growth rate cannot be too large, the number of elements in the aquifer is also impacted by the element size inside the pipe.

Line elements are computationally more efficient, but simplified flow equations must be used. It has been shown that, when using line elements, the hydraulic gradient at the tip of the pipe overestimates the experimental gradient (Robbins et al., 2022). In a 3D simulation using 2D plate elements, a reduced flow rate within the pipe was observed (Bersan et al., 2013). This may be caused by the reduced dimension of the pipe, especially since the effect decreases with a coarser mesh and smaller aquifer depth.

Overcoming the scale difference of the micro-scale pipe(-tip) in a macro-scale aquifer is a significant challenge in continuum modelling, since the transition from the aquifer to the pipe leads to a singularity at the tip of the pipe. One way to better represent the flow at the tip of the pipe is to create an extremely fine mesh at the layer where piping is expected to occur; however, this will lead to large computational efforts. Robbins and Griffiths (2021a) propose an adaptive meshing strategy to better represent flow at the pipe tip without requiring an overly fine mesh in the area where the pipe is not present. Several numerical methods, though not yet applied in BEP modelling, may offer potential solutions to the singularity issue at the pipe tip. These include: xFEM which is used in the numerical modelling of crack propagation (Li et al., 2018); multigrid methods such as applied in fracture flow modelling and computational fluid dynamics (CFD) (Arrarás et al., 2019), and meshless methods such as smooth particle hydrodynamics (SPH) as was applied in internal erosion modelling (Nguyen et al., 2008; Ma et al., 2024).

BEP is often modelled as a 2D cross-section. However, over the past decade it has been shown that 3D approaches yield significantly different results compared to 2D models. Due to the convergence of flow at the pipe tip, the flow rate inside the pipe in 3D situations is significantly larger than in 2D situations (Vandenboer et al., 2014; Van Beek et al., 2022). If multiple pipes grow at a close distance from each other, the 2D approach may be valid. However, it is difficult to predict whether a single pipe or multiple pipes will grow in a field situation. Since the 2D cross-section model does not consider meandering or branching of the pipe, 2D plan view models have been created as well (Kanning and Calle, 2013; Robbins et al., 2021). Fig. 4 shows the development of 2D vs. 3D models over the past decades. Prior to 2012, only three papers presented numerical models of BEP—two using 3D approaches and one using a 2D approach. Since 2012, 2D models have expanded with different capabilities. While fewer 3D models were developed prior to 2018, recent years have seen a shift, with more 3D models being published than 2D models.

Because continuum methods can still be computationally expensive, machine learning techniques have been combined with numerical methods (Sellmeijer, 2006; Kaunda, 2015; Aguilar-López et al., 2016; Fascetti, 2022). This technique enables a large number of cross-sections to be analysed efficiently, which is required to design and assess long stretches of dikes.

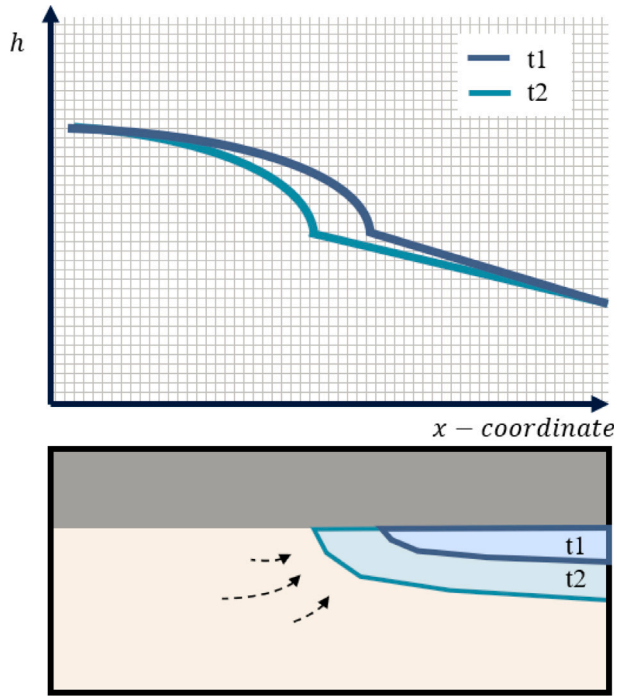

Fig. 5. Pipe development over time in a progression dominated situation (t1–t2), before the critical pipe length is reached. Because the flow towards the tip becomes less concentrated, due to the lengthening of the pipe and the flow directly entering the body of the pipe, the hydraulic gradient $\Delta h/\Delta x$ in front of the pipe tip decreases. This combined with deepening of the pipe leads to decrease of the hydraulic gradient inside of the pipe.

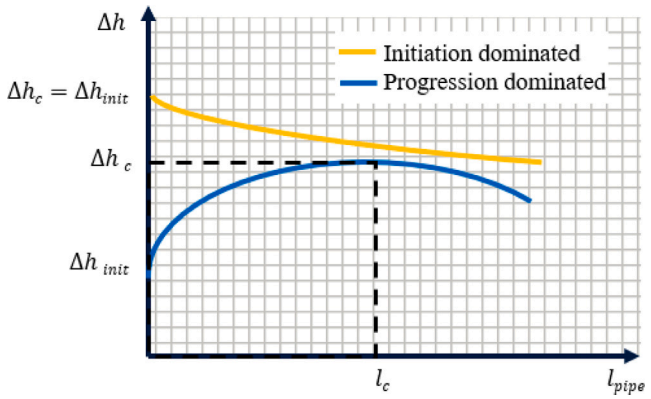

Fig. 6. Equilibrium theory based on (Van Beek, 2015). When piping is progression dominated piping can occur and stabilize until the critical pipe length l_c. When the critical head difference is exceeded, the pipe progresses to the upstream side if the head difference remains constant. In initiation dominated situations the head difference at which piping is initiated is also the critical head, meaning the pipe will progress to the upstream side if the head remains constant. Van Beek (2015) demonstrated this experimentally by lowering the applied head difference to 0 after initiation and reapplying a head until pipe progression continued.

2.2. Temporal scale

Numerical models can be either steady-state, quasi-steady-state or time-dependent.

Steady-state models are used to study specific aspects of BEP. However, they are not suited for the determination of the critical head, unless an iterative approach is applied to determine the equilibrium conditions for all given pipe lengths and depths (Aguilar-López et al., 2016). Steady-state BEP models have been used to study the validity of the cubic law (Bersan et al., 2013), the influence of 3D groundwater flow (Vandenboer et al., 2014), the influence of existing structures in the foundation of the dike on BEP (Aguilar-López et al., 2016) and different sandboil/pipe configurations (Navin and Shewbridge, 2017).

Quasi steady-state models have a primary erosion criterion, a secondary erosion criterion or both. The hydraulic head at the upstream water level is increased step-wise to determine the critical head at which the pipe grows to the upstream end. Equilibrium can occur depending on the outflow configuration. If a blanket layer is present and a single sandboil forms, or if there is a narrow ditch, equilibrium is likely to occur. Consequently, when there is no blanket layer, equilibrium is less likely to occur, especially for small spatial scales. This can be explained by the redistribution of flow as the pipe progresses. When a pipe initiates from a sandboil, the concentration of flow towards the pipe tip is large. As the pipe progresses, groundwater flow redistributes along its length and becomes less concentrated towards the pipe tip, thus reducing the load on the tip (see Fig. 5). Similarly, secondary erosion is reduced by the progression of the pipe. This is due to the fact that, as the pipe gets longer, it also deepens, thereby reducing the tangential flow velocity inside the pipe and secondary erosion. The pipe growth process is shown in Fig. 6.

Interestingly, Wang et al. (2014) observed the following from their simulations: "for the case without a cut-off wall, the simulation shows that if the water head exceeds the critical value, piping erosion will occur and continue to progress until it reaches the upstream boundary". However, when looking at the observations from the experiments as described by Zhou et al. (2012), equilibrium was found. This discrepancy may be caused by the primary erosion criterion that was applied, or by an underestimation of the flow resistance inside the pipe. If significant resistance exists within the pipe, equilibrium may still occur even when only a primary erosion criterion is applied. This occurred in the simulations by Robbins (2016). To estimate the flow resistance in the pipe, incorporating a secondary erosion criterion is advisable.

Models with primary erosion criteria can be used to study the meandering of the pipe (Kanning and Calle, 2013) and give an impression of the influence of cut-off walls and other remedial measures (Wang et al., 2014; Robbins and Griffiths, 2021b). BEP can be either initiation or progression dominated, depending on the type of exit configuration and scale of the experiment (Van Beek et al., 2014). In progression dominated situations, the initial concentration of groundwater flow towards the exit configuration leads to the initiation of piping. However, as the pipe lengthens and deepens, the groundwater flow and pipe flow get redistributed leading to a reduced load on the sand grains. This redistribution may lead to equilibrium, which can persist until the pipe reaches the critical pipe length (l_c [m]) (see Fig. 6). In initiation dominated situations the upstream hydraulic head required for initiation of BEP is equal to the critical head. As the pipe progresses, the required hydraulic head for the pipe to progress further decreases.

The secondary erosion criterion is expressed as a critical value (e.g. flow velocity, shear stress, hydraulic gradient), which, if exceeded, causes the removal of grains from the bottom and walls of the pipe and the subsequent deepening and widening of the pipe. As the pipe widens and deepens, flow velocities decrease, thus reducing the transport capacity in the pipe and potentially leading to an equilibrium. Equilibrium models use a secondary erosion criterion and are sometimes combined with a separate progression criterion to facilitate the iterative progression (Sellmeijer, 2006; Esch et al., 2013; Zhou et al., 2012; Robbins and Griffiths, 2021a). The interaction between primary and secondary erosion in the numerical modelling of BEP has not yet been studied in detail.

Time-dependent models couple groundwater flow with sediment mass conservation. DEM models are always time-dependent due to the equations of motion, which govern the movement of the particles. Time-dependent pipe progression is achieved through transport

equations, which can be either for primary erosion (Fujisawa, 2016), secondary erosion (Wewer et al., 2021; Pol et al., 2024) or both (Rotunno et al., 2017, 2019). The time-dependent models can be calibrated on BEP experiments (Rotunno et al., 2019; Callari and Pol, 2022) or existing transport equations based on flume experiments are used in BEP modelling (Wewer et al., 2021). Pol et al. (2024) used a transport equation specifically corrected for BEP modelling.

Most backward erosion piping models do not consider the initiation (uplift/heave) and failure of the water retaining structure (stability); however, a few exceptions exist (Rahimi and Shafieezadeh, 2020; Zhang et al., 2022; Ma et al., 2024). Instead BEP is modelled as the growth of the pipe from downstream to upstream. The models assume initiation occurs instantaneously and that failure of the dike is imminent when the pipe reaches the upstream side.

2.3. Application

At all spatial and temporal scales, validation and calibration are an issue due to a lack of micro-scale measurements of the macro-scale process. Table 1 shows the number of experiments used to validate the numerical models. The more complex models generally have more parameters, but not all experiments have suitable measurements for the calibration of numerous parameters and opportunities for independent validation have been rare or non-existent. However, simple models cannot capture the complex 3-dimensional time-dependent process and might generalize the problem too much.

The existing numerical BEP models use different software tools, some of which are commercial and require licences, whereas others are custom-made codes. Commercial geotechnical programs that are used for BEP modelling are PLAXIS (Brinkgreve et al., 2016), SEEP/W (GEO-SLOPE International, 2015), FLAC3D (Itasca Consulting Group, 2023) and iMOD (Vermeulen, 2013). With the exception of iMOD, there are licence costs for using these programs. A great advantage of these types of models is the relative ease of use and the use of validated governing equations. However, the flexibility of these programs is limited and therefore it is challenging to capture the full BEP process with these types of models.

General finite element solver software such as FEAP (Taylor, 2014), COMSOL Multiphysics ® (COMSOL AB, 2024) and Abaqus (Smith, 2009) has also been used to model BEP. The main advantage of using general finite element software is the relative flexibility of being able to solve differential equations of your own choosing. All these programs are available upon payment for the licence.

Custom codes (as well as DgFlow) are often tailored for BEP modelling and therefore cannot be used for other applications. Often the code will be available upon request or in collaboration with the creators; however, this is at the creator's discretion.

The program MSeep was discontinued and replaced with the freely accessible D-Geo Flow (Van der Meij, 2024), which is a 2D FEM BEP program.

3. Flow modelling

During BEP, two flow domains can be distinguished, the porous aquifer and the hollow erosion channel. In the modelling of BEP, different (sets of) equations are used to calculate the flow in these domains. The governing equations used to model flow in BEP greatly impact the discretization and therefore the computational effort and the capabilities of the model. The advantages and disadvantages of each modelling approach are shown in Table 2.

3.1. Groundwater flow

Groundwater flow is commonly represented as a combination of Darcy's law Eq. (1) and the conservation of mass Eq. (2).

$$u = -k\nabla h \tag{1}$$

$$S_s \frac{\delta h}{\delta t} = -\nabla u \tag{2}$$

In these equations, S_s [m^{-1}] represents the specific storage, u [m/s] the Darcyan velocity, and k [m/s] the hydraulic conductivity. In groundwaterflow modelling, the Darcyan velocity is commonly represented by q. When the porosity is 1 [–], the Darcyan velocity equals the flow velocity. The total head h [m] is defined as $h = \frac{p}{\rho_w g} + z$, where p [Pa] is the pressure, ρ_w [kg/m^3] the density of water and g [m/s^2] the gravitational acceleration. Darcy's law is valid for laminar conditions. Starting at Reynolds numbers larger than 1–10 inertial effects become significant (Bear, 1972). Therefore the Forchheimer equation may perform better than Darcy's law in situations with high flow velocities. [Note: the Reynolds number in this statement is defined as $Re_D = \frac{qd}{\nu}$, where d [m] is a characteristic length which has been defined by various authors between d_{10} and the mean grain size, ν is the kinematic viscosity of the fluid]. In flows along the interface between open channels and porous media, or in aquifers with preferential flow paths Darcyan flow cannot be applied (Jennings and Pisipati, 1999). Brinkman (1949) developed an alternative equation with which these interface flows can be resolved. The combined Brinkman–Forchheimer (BF) equation is shown in Eq. (3).

$$\nabla p - \mu'\nabla^2 u + \frac{\mu}{\kappa}u + \beta\rho_w u^2 - F = 0 \tag{3}$$

In this equation, μ' [kg/(m s)] is the effective viscosity (it is often assumed equal to the viscosity μ) and κ [m^2] is the intrinsic permeability of the soil, which is related to the hydraulic conductivity as $\kappa = k\mu/(\rho g)$. The Forchheimer term $\beta\rho_w u^2$ accounts for inertial effects, in which β [1/m] is an empirically determined coefficient. F is a vector to account for volume forces such as gravity. It is usually not included in the brinkman equation, but (Bersan et al., 2013) used this term in BEP modelling. The Brinkman term $\mu\nabla^2 u$ represents diffusion. When the permeability in Eq. (3) is large, the equation represents laminar open/conduit flow; when the permeability is small the equation approximates groundwater flow. Therefore, the Brinkman–Forchheimer equation can represent the flow in both the porous medium and the conduit.

3.2. Free fluid flow

Free fluid flow can be modelled using continuum methods such as FDM or FEM of the Navier–Stokes equations or using the Lattice-Boltzmann method. Fluid flow occurs both in the aquifer and in the pipe, although there is more resistance to flow in the aquifer due to the soil skeleton. In BEP models that use DEM, free fluid flow modelling is used in the entire domain to compute the flow velocities and pressures. Fluid flow is governed by the conservation of mass, momentum and energy. The convective form of the incompressible Navier–Stokes (NS) equations is shown in Eqs. (4)–(5); these are derived from the conservation of mass and momentum.

$$\nabla \cdot u = 0 \tag{4}$$

$$\rho_w\left(\frac{\partial u}{\partial t} + (u\cdot\nabla)u\right) = \mu\nabla^2 u - \nabla p + \rho_w f_i + \rho_w g \tag{5}$$

In these equations, f_i [m/s^2] is any forcing/resistance term that can be added. In BEP modelling (Shamy and Aydin, 2008; Wang and Ni, 2013; Nie et al., 2022), the Ergun equation (Ergun, 1952) Eq. (6) and the Di-Felice equation (Di Felice, 1994) Eq. (7) have been used

Table 2
Comparison flow modelling.

Aquifer flow	Pipe flow	Advantage	Disadvantage	Nr. of models
Free fluid flow	Free fluid flow	Physics based	Extremely computationally expensive	5
BF	BF/NS	Physics based	Computationally expensive, regression based erosion laws	2
Darcy	1D pipe flow	Experimentally validated, computationally cheap	Many assumptions and calibration factors, simplification of physics	18
Darcy	Darcy	Computationally cheap	Uncertainty of the permeability increase may lead to large errors in the head loss in the pipe	12

as resistance terms to represent the soil-fluid interaction. The Ergun resistance term is similar to the Brinkman–Forchheimer equation.

$$f_{Ergun} = \left(150\frac{(1-n)^2}{n\rho_w d^2}\mu + 1.75\frac{(1-n)|\Delta v|}{d}\right)\Delta v \tag{6}$$

$$f_{Di-Felice} = \frac{1}{2}C_d\pi\left(\frac{d}{2}\right)^2 \Delta v|\Delta v| \cdot n^{1-\chi} \tag{7}$$

In these equations, d [m] is the grain diameter and Δv [m/s] the difference in flow velocity between the particle and the fluid. Similar to Eq. (3), the Ergun equation includes the pressure loss due to inertia. In the Di-Felice equation, C_d is the drag coefficient and χ is an empirical correction factor.

As an alternative to solving NS using continuum methods, the flow in the aquifer and pipe has been computed using the Lattice-Boltzmann method (Perumal and Dass, 2015) in combination with DEM for BEP modelling (Tran et al., 2017; Froiio et al., 2019). In this approach, the fluid density is simulated in collision and streaming steps. In streaming steps, fluid moves to neighbouring nodes on the lattice, and in each collision step the incoming fluid is redistributed according to the local equilibrium distribution function Eq. (8).

$$\begin{aligned} f_\alpha^c(x,t) &= f_\alpha(x,t) - \frac{\Delta t}{\tau_f}(f_\alpha(x,t) - f_\alpha^{eq}(x,t)) \\ f_\alpha(x + e\Delta t, t + \Delta t) &= f_\alpha^c(x,t) \end{aligned} \tag{8}$$

In these equations, $f_\alpha^c(x,t)$ is the density component in direction α at the location x and time t, the index c refers to the post-collision state. The parameter e is the velocity, τ_f is the relaxation time and Δt is the time step. In comparisons between NS solved with FEM and LBM, it is demonstrated that similar accuracy can be achieved (Kandhai et al., 1998; Geller et al., 2006; Schlauch et al., 2013). These comparative studies reached different conclusions on what the more computationally efficient approach is. The most efficient approach may depend on the application. There is no comparative study oriented at BEP modelling.

In BEP models that use DEM, either a continuum method to solve NS or LBM is applied. Both NS and LBM are computationally expensive to solve; therefore, these approaches are not widely applied in engineering practice. As shown in Table 2, there are only 5 models that apply DEM modelling. The advantage of this type of flow modelling is that the fundamental physics is accurately represented, with few simplifying assumption. BEP models that use (variations of) the BF equation represent the pipe using (variations of) the NS equations (Bersan et al., 2013; Fujisawa, 2016). However, including the convective term $((u\cdot\nabla)u)$ of the NS equation has been criticized in combination with the Forchheimer term (Nield, 1991), because of its overestimation of inertia in the porous media domain. Additionally, the BF equation is intended for high-porosity/high hydraulic conductivity soils ($n > 0.6$, $n[-]$ is the porosity) (Joseph et al., 1982; Nield, 1991).

3.3. Headloss in the pipe

To reduce the computational effort of flow modelling in BEP, the flow inside of the erosion channel is often simplified using 1D pipe flow equations. These equations are steady-state approximations and assume that the impact of lateral influx on the shear stress is negligible. The impact of the steady-state assumption for pipe flow has not been studied for BEP. During pipe progression, the flow at the pipe tip will accelerate. The assumed steady-state flow velocity is larger than the accelerating flow velocity; therefore, erosion rates may be overestimated at the tip of the pipe. Models that combine Darcyan flow with 1D pipe flow equations are the most common in BEP modelling (Table 2). The Darcy–Weisbach equation as shown in Eq. (9) is one example of such a head loss equation.

$$\frac{\delta h}{\delta x} = f\frac{u^2}{2gD_h} \tag{9}$$

In this equation, the head gradient $\frac{\delta h}{\delta x}$ is a function of $f[-]$ which is a friction factor that depends on the fluid properties, the geometry and roughness of the conduit. The hydraulic diameter is D_h [m] and g [m/s^2] is the gravitational acceleration. Slightly different versions of this equation are also used (Zhou et al., 2012; Wang et al., 2014). In case of laminar flow, the friction factor only depends on the flow itself and the geometry of the pipe; see Eq. (10).

$$f = \frac{\beta_{geom}}{Re} \tag{10}$$

The Poiseuille number $\beta_{geom}[-]$ is a cross-section-dependent variable and Re is the Reynolds number. Inserting Eq. (10) into Eq. (9) results in Poiseuille's law. Because both Poiseuille's law and Darcy's law show a linear relationship between flow velocity and pressure gradient, the friction can be rewritten as an equivalent permeability. The resulting expression for the equivalent permeability (11) is derived by combining Eqs. (1), (9) and (10) This expression is often used in BEP modelling (Bersan et al., 2013; Esch et al., 2013; Aguilar-López et al., 2016; Robbins and Griffiths, 2021a; Wewer et al., 2021):

$$\kappa_{eq} = \frac{2D_h^2}{\beta_{geom}} \tag{11}$$

If the flow is turbulent, wall friction is of great importance. There is no expression for an equivalent permeability in turbulent flow, because the correlation between the pressure gradient and flow velocity is not linear; therefore, this has to be solved implicitly. The empirical Moody-Diagram (Moody, 1944) can be used to derive the friction factor; however, in numerical modelling this is difficult to apply. In BEP modelling, Robbins and Griffiths (2021a) used the explicit relation by Romeo et al. (2002) Eq. (12) to determine the turbulent friction in the pipe.

$$\begin{aligned} \frac{1}{\sqrt{f}} = -2log_{10}\Bigg(\frac{\frac{\epsilon}{Dh}}{3.7065} - \frac{5.0272}{Re}log_{10}\Bigg(\frac{\frac{\epsilon}{Dh}}{3.827} - \\ \frac{4.567}{Re}log_{10}\Bigg(\Bigg(\frac{\frac{\epsilon}{Dh}}{7.7918}\Bigg)^{0.9924} + \Bigg(\frac{5.3326}{208.815+Re}\Bigg)^{0.9345}\Bigg)\Bigg)\Bigg) \end{aligned} \tag{12}$$

Similarly Okamura and Kusube (2025) assumed the following relation for turbulent pipe flow:

$$\frac{1}{\sqrt{f}} = -2log_{10}\left(\frac{2d}{Dh}\right) + 1.74 \tag{13}$$

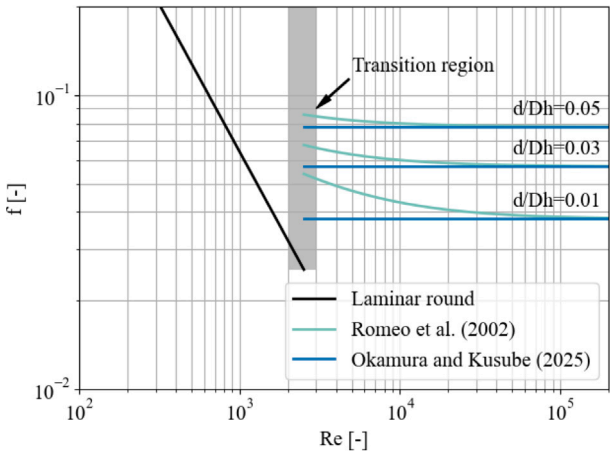

Fig. 7. Moody diagram with different equations to determine the Darcy–Weisbach friction factor.

Eqs. (10), (12) and (13) are shown in the Moody diagram in Fig. 7. Eq. (12) converges towards Eq. (13) for high Reynolds numbers. And when the grain-size to pipe depth ratio is large, the difference in friction is small. For smooth pipes, Eq. (13) underestimates the friction in the pipe. However, smooth pipes are unlikely to occur in BEP, especially in combination with small Reynolds numbers.

Alternatively the friction factor can be an input parameter chosen by the user (Rotunno et al., 2019).

The flow regime inside the pipe is determined by means of the dimensionless Reynolds number Eq. (14)

$$Re = \frac{\rho u D_h}{\mu} \tag{14}$$

The critical Reynolds number, beyond which flow can no longer be considered laminar, for circular pipes is approximately 2300 (Pritchard and Mitchell, 2016), whereas the critical Reynolds number for parallel plates is 2800 (Tosun et al., 1988; Hanks and Ruo, 1966).

Most authors assume laminar flow because of its relative simplicity and because in some small-scale experiments with injected dye, limited mixing was observed and the Reynolds number was relatively low (order of $\approx 10^2$) (Robbins and Van Beek, 2017; Van Beek et al., 2019). However, at large-scale or field-scale, the pipe dimensions and flow regime are unknown. In centrifuge experiments, Reynolds numbers exceeding the critical Reynolds number have been observed (Okamura et al., 2022). It has been shown in a 2D top view model, that even with a low permeability sand (with a hydraulic conductivity of $k = 10^{-5}$ m/s), Reynolds numbers exceeding the critical value can occur in BEP when the aquifer depth is large (Robbins and Griffiths, 2021a). These calculations, which assumed turbulent pressure loss in the pipe, resulted in a slightly lower critical head, although the difference was small. When laminar flow is assumed, but the flow is turbulent, the friction in the pipe is underestimated. Therefore, the hydraulic gradient in the pipe will be smaller and the critical head will be overestimated if laminar flow is assumed.

In 1D pipe flow equations, the impact of the lateral influx on the acting shear stress is assumed to be negligible. In a comparative study between Hagen–Poisseuille and Stokes flow, in which a small-scale BEP experiment was modelled, the difference between the approaches was negligible (Bersan et al., 2013). However, in the model by Xiao et al. (2023), which assumes laminar flow, the lateral influx is explicitly included in the friction coefficient based on the empirical model by Ouyang et al. (1998); their model shows a significant increase of the hydraulic gradient where the lateral influx is largest.

$$f_{total} = f_{tangential}(1 + 0.043 Re_w^{0.6142}) \tag{15}$$

In this equation, the tangential friction factor $f_{tangential}$ equals the laminar friction factor of Eq. (10) and $Re_w = \frac{\rho_w u_p 2d}{\mu}$ is the inflow Reynolds number based on the lateral inflow velocity u_p. In case of turbulent flow, the friction factor tends to decrease with a lateral influx (Ouyang et al., 1998; Cheng and Chiew, 1999; Francalanci et al., 2008; Lu et al., 2008).

A common assumption is that there are no additional pressure losses due to cross-section fluctuations and meandering of the pipe. Pressure losses due to meandering and cross-section fluctuations were accounted for in one model (Wewer et al., 2021) by applying correction coefficients; however, validation of these coefficients is lacking.

As shown in Table 2, this type of modelling is the most common. Consequently, it is also the most calibrated and validated modelling method, but models in this category struggle with accurately representing the large-scale, 3D, time-dependent process of BEP without calibration (Pol et al., 2024; Callari and Pol, 2022). It is expected that this deviation is caused by previously mentioned assumptions, which may not hold up in large-scale experiments, and the experimental calibration which is performed using mostly small-scale experiments.

3.4. Darcyan pipe flow

Models which increase the hydraulic conductivity of the pipe(zone) with a given parameter $C[-]$ with respect to the aquifer are essentially a Darcyan seepage flow analysis. The equation to increase the hydraulic conductivity is Eq. (16).

$$\kappa_{eq} = C\kappa \tag{16}$$

This increase coefficient $C[-]$ ranges from 5 to 20,000 (Ding et al., 2007; Kanning and Calle, 2013; Robbins, 2016; Fascetti and Oskay, 2019a). Alternatively, the value of κ_{eq} can be directly assumed (Barendsen, 2020). With calibration, a critical head similar to experiments may be obtained, but the model cannot be scaled or extrapolated. Therefore, this type of models are more suitable for qualitative or comparative studies.

Alternatively, the increase in hydraulic conductivity can be calculated based upon the increase in porosity (Liang et al., 2017; Rahimi et al., 2021; Fascetti and Oskay, 2019b). In this approach fine grains are eroded from the soil skeleton due to seepage flow. The porosity and hydraulic conductivity increase because of this. The process described with this type of modelling is more similar to suffusion than BEP, because no hollow conduit is created.

4. Erosion

Erosion in BEP is subdivided into primary erosion (at the tip of the pipe) and secondary erosion (in the body of the pipe). Erosion leads to the growth (lengthening, deepening, widening) of the pipe. The onset of motion criterion defines whether erosion is occurring and transport equations determine the amount of erosion. As shown in Fig. 8, 17 models have an onset of motion criterion without transport equations, most of these models are quasi-steady-state. To model time-dependent BEP, transport equations are required; these generally depend on the amount by which the load exceeds the onset of motion criterion. Currently, 12 BEP models have transport equations. The other 8 models are either steady-state or use erosion laws better suited for other types of internal erosion. In Table 1 the erosion type per model can be found.

4.1. Primary erosion

Currently, there are three main groups of primary erosion criteria. Each of these criteria uses a quantity proportional to the hydraulic gradient to assess if primary erosion is occurring. The different primary erosion methods are explained below and visualized in Fig. 9.

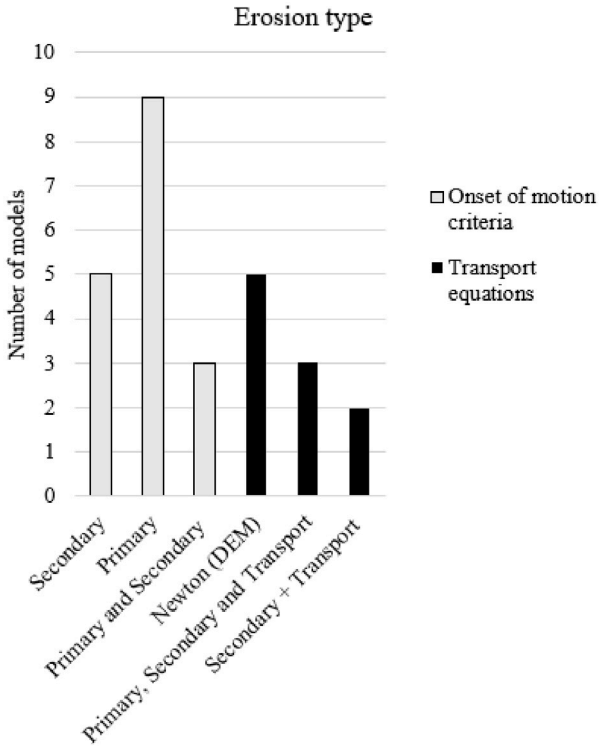

Fig. 8. Overview of erosion types applied in BEP modelling. SE and PE are secondary erosion and primary erosion respectively. In DEM models, Newton's law is applied to determine the displacement of grains. T refers to the presence of transport equations.

1. Critical secant gradient: In this method, a critical (secant) gradient in front of the pipe tip is established and, if exceeded, the pipe progresses. The critical secant gradient in front of the pipe tip can be determined experimentally. However, due to the meandering nature of BEP and the limited number of pressure sensors in an experiment, measuring the tip gradient is difficult. Experiments that constrain the pipe along a given path, thereby limiting the meandering, have been used to determine the critical secant gradients. Critical secant gradients ranging between 0.2 and 1.5 have been found experimentally (Xiao et al., 2019; Pol et al., 2022; Robbins, 2022). The critical secant gradient depends on the length over which it is determined. To overcome this length effect of the critical secant gradient, Robbins and Griffiths (2022) developed the critical secant gradient function (CSGF) similar to the derivation for the head profile in front of the pipe tip by Xiao et al. (2019).

$$i_{cs,tip} = \frac{C_{CSGF}}{\sqrt{x_{tip}}} \tag{17}$$

The material factor $C_{CSGF}[\sqrt{m}]$ depends on the grain size, the uniformity coefficient and the void ratio and x_{tip} [m] is the upstream distance from the pipe tip. With the CSGF, the critical secant gradient measured at a small-scale can be translated to the critical secant gradient over a larger distance, which is easier to implement in numerical modelling.

2. Collapse of the pipe tip: In this conceptualization it is assumed that the gradient in front of the pipe tip is always sufficient to lead to the collapse of the pipe tip. However, this collapse leads to the deposition of sand grains at the bottom of the pipe tip (Pol et al., 2022). Due to this collapse and deposition, the erosion channel is narrower at the tip, causing the pressures to rise at the tip. Because of these increased pressures, the gradient at the tip is smaller and the progression stops until the collapsed grains are transported from the bottom of the pipe tip. Only then can progression occur again Pol et al. (2022). In this conceptualization, the pipe progression is strongly influenced by secondary erosion because this leads to the removal of grains at the bottom of the pipe tip. This theory fits with the experimental occurrence of an equilibrium and is supported by the strong correlation found between the progression rate and the shear stresses at the bottom of the pipe tip (Pol et al., 2022). Models in which only secondary erosion is used to determine if progression occurs (Sellmeijer, 2006; Esch et al., 2013; Wewer et al., 2021) imply this conceptualization. In case of barriers in the pipe path or highly heterogeneous soils, this method is less suitable because in these situations the collapse of the tip may not occur, even when grains from the bottom of the pipe tip have been removed. The direction of propagation of the pipe tip cannot be determined accurately without a criterion in front of the pipe tip.
3. Increased porosity: Another conceptualization of the tip progression is that, due to the concentration of flow towards the tip of the pipe, the porosity increases. This can be explained by the removal of fine grains from the soil skeleton (Rotunno et al., 2019; Wang et al., 2014). Some authors observed the rearrangement of fine grains in front of the pipe tip (Pol et al., 2022; Vandenboer, 2019). The erosion of fine grains is based on the exceedance of an onset of motion criterion which differs per author. The removal of fine grains leads to an increase in porosity in front of the pipe tip. This increase in porosity causes an increase in hydraulic conductivity; often the Kozeny–Carman relation (Carman, 1956) is used to relate the porosity to the hydraulic conductivity. After an assumed (or calibrated) critical value for the porosity in front of the pipe tip is reached, the tip collapses and the pipe progresses.

Primary erosion can be implemented in three different ways in the numerical modelling of BEP. (I) The pipe has a fixed (straight) path and primary erosion leads to the lengthening along this path (Rotunno et al., 2019). (II) The pipe chooses the path of least resistance. This results in a single meandering pipe (Kanning and Calle, 2013) in a heterogeneous field or a pipe progresses downward underneath a barrier (Wang et al., 2014). (III) The pipe can progress in any direction exceeding the critical gradient. This allows for both meandering and branching of the pipe (see Fig. 1) (Robbins and Griffiths, 2021a; Rahimi et al., 2021).

DEM studies have shown that there is an arching effect (Fang et al., 2020) in front of the pipe tip, which may be one of the causes for resistance of the pipe tip against primary erosion (Tran et al., 2017; Froiio et al., 2019). However, the conditions under which this arching effect occurs are not yet fully understood. In a 3D macro-scale CFD-DEM model, Nie et al. (2022) concluded that increasing hydraulic gradients leads to a greater range of contact forces between particles with depth. In addition to the horizontal seepage forces of primary erosion, vertical seepage forces may also be important in the progression of the pipe tip. Vertical seepage flows may weaken the tip due to the strong concentration of flux, and associated heave can result in a deep/rounded pipe tip shape (Hanses, 1985; Schmertmann, 2000; Allan, 2018; Xiao et al., 2019). Contrary to this deep pipe tip, a shallow pipe tip with a gradual slope is also observed in small scale experiments (Vandenboer et al., 2019; Pol et al., 2022). Additionally, vertical seepage flow is relevant to flow around vertical barriers, such as sheet pile walls. To study the impact of vertical seepage on BEP, experimental research can be combined with DEM modelling.

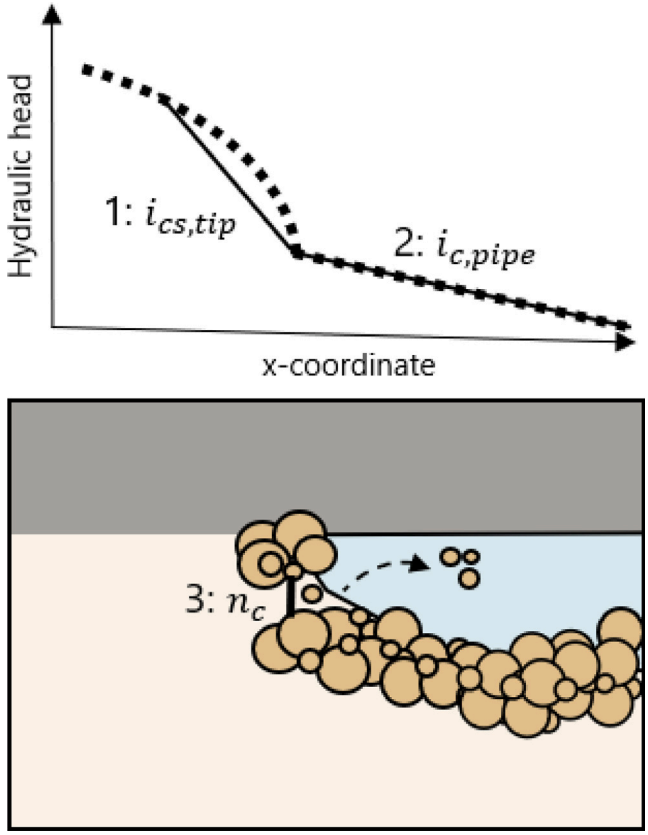

Fig. 9. Primary erosion modelling methods. 1: the critical secant gradient, 2: collapse of the pipe tip, 3: increased porosity.

4.2. Secondary erosion

Secondary erosion is caused by tangential flow along the bottom and walls of the pipe, which leads to the deepening and widening of the pipe. Erosion occurs when the forces (e.g. drag, lift, gravity) acting on a grain are out of equilibrium. It is often expressed in terms of an onset of motion criterion which has to be surpassed. The driving forces are expressed as a function of either the hydraulic gradient i[−] the shear stress τ [kN/m^2], the Shields parameter Θ[−] or the flow velocity u [m/s]. These parameters can be related to each other using Eqs. (18), (19) and (20).

In steady-state conditions, the shear stress can be derived by the equilibrium of forces in a cross-section. The shear stress is linearly correlated to the hydraulic gradient inside the pipe i_{pipe}.

$$\tau = \frac{Dh}{4}\rho_w g i_{pipe} \tag{18}$$

In this equation the hydraulic diameter is Dh [m]. In a parallel plate geometry, which is often assumed in BEP modelling, $Dh = 2a$, where a is the depth of the pipe.

The flow velocity u can be related to the critical shear stress using the following expression, as was derived by Pol et al. (2022) based on (Sellmeijer, 1988) and Spiga and Morino (1994).

$$\tau_{u,a} = \frac{6\mu u}{a} \tag{19}$$

The critical shear stress (τ_c) can be expressed as critical Shields parameter (Θ_c), which is defined as:

$$\Theta_c = \frac{\tau_c}{(\rho_s - \rho_w)gd} = func\left(Re_*\right) \tag{20}$$

In this equation, ρ_s is the density of the grains. The function $func()$ was originally not defined but, instead, experimental results were directly plotted on the Shield diagram (Fig. 10). The particle Reynolds number is defined as $Re_* = \frac{u_* d}{\nu}$. Its value indicates whether the hydraulic conditions are smooth (the grain experiences only laminar flow) or rough (the grains protrude the laminar sub-layer and experience turbulent flow). As such, the Shields diagram can visualize the impact of different hydraulic regimes on the sediment transport. The particle Reynolds number depends on the dimensionless shear stress ($u_* = \sqrt{\frac{\tau_b}{\rho_w}}$). Because the particle Reynolds number depends on the shear stress, the formulation is implicit and requires an iterative approach to find a solution. Alternatively, the Shields diagram can be expressed by the dimensionless grain size $D^* = d_{50}\sqrt[3]{\frac{\Delta g}{\nu^2}}$ (Van Rijn, 1984). An advantage of expressing the Shields parameter as a function of the dimensionless grain size is that the formulation is explicit. The particle Reynolds number and the dimensionless grain size are related through the following expression: $Re_* = \sqrt{D^{*3}\Theta_c}$.

There are many different methods to determine the onset of motion criterion. Most depend on the grain size and weight of the soil, as well as the loading conditions. Several of these methods are shown in Fig. 10. The explicit relation by Cao et al. (2006) is included as reference because it covers both the hydraulic smooth (left side of the figure) and hydraulic rough (right side of the figure) regime.

One of the onset of motion criteria used in BEP modelling is $\tau_c = d_{50}$ (Briaud et al., 2017). This empirical relation where d_{50} is in millimetres is used by Robbins and Griffiths (2021a) [Note: the units are inconsistent, τ_c is in N/m^2]. Because τ_c is linearly correlated to the grain size in this criterion, the Shields parameter is independent of grain size (see Eq. (20) and Fig. 10). Robbins (2022) improved the empirical onset of motion criterion by Briaud et al. (2017), by adding an exponent $\tau_c = d_{50}^{0.8}$. Another linear correlation between the grain size and critical shear stress was derived by White (1940) and is applied in several models (Sellmeijer, 2006; Esch et al., 2013; Aguilar-López et al., 2016). The shear stress over a grain is integrated over the surface area and the resistance force is due to gravity and the interlocking of the grains. The critical shear stress according to White is:

$$\tau_c = \eta\frac{\pi}{6}\rho' g d_x tan(\theta) \tag{21}$$

In this equation $\rho' = \rho_s - \rho_w$ is the effective density of a submerged particle. White's coefficient $\eta = 0.25$ [-] and the bedding angle $\theta = 37°$ were chosen as conservative values by Sellmeijer based on the large BEP flume experiments (Silvis, 1991) [Note: originally there were two coefficients, α and η, in White (1940) but in BEP modelling they are assumed as a single parameter η since the work by Sellmeijer and Koenders (1991)]. The suitability of White's criterion for BEP is a subject of debate (Pol, 2020) since it was originally based on a limited range of experiments and because it shows a poor fit with other experiments (see the green dotted line in Fig. 10). White's expression for the critical shear stress was extended based on a larger range of laminar flow flume experiments (Van Beek, 2015). This resulted in an alternative expression for $\theta = 8.125ln(d_{50}) - 38.777$, in which White's coefficient is $\eta = 0.3$ and the grain size is defined as the 50 percentile grain size $d_x = d_{50}$ [m]. This expression is shown as the green dashed line in Fig. 10.

A multivariate calibration of Sellmeijer's semi-analytical model based on experimental data resulted in a revised calculation rule (Sellmeijer et al., 2011). In this rule an additional calibration coefficient for the grain size of $\left(\frac{d_{70}}{d_{70,m}}\right)^{0.6}$ was introduced, where $d_{70,m}$ denotes the median grain size used in the calibration experiments. There is no physical explanation for the calibration coefficient; it may be caused by vertical seepage in BEP or by non-laminar flow inside the erosion channel. By assuming this coefficient is erosion-related and adding this coefficient to Eq. (21), this results in Eq. (22), as was done by Van Beek (2015) and Van Beek et al. (2022).

$$\tau_c = \eta\frac{\pi}{6}\rho' g d_x tan(\theta)\left(\frac{d_{70}}{d_{70,m}}\right)^{0.6} \tag{22}$$

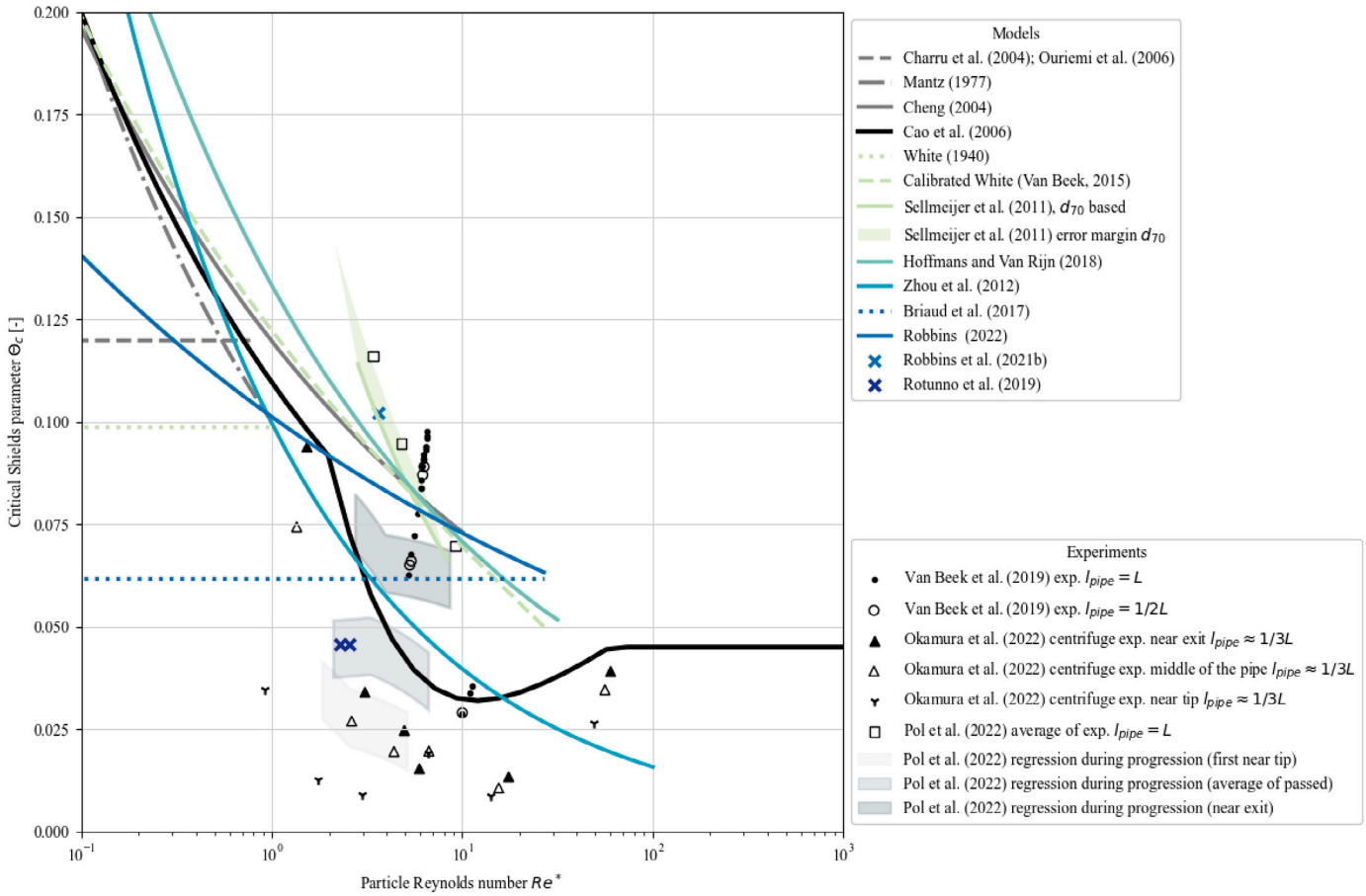

Fig. 10. Secondary erosion criteria plotted on the Shields diagram. The model by Cao et al. (2006) has not been used in BEP modelling but is added because it shows a wider range over the Shields diagram. Sellmeijer et al. (2011) and Hoffmans and Rijn (2018) are part of (semi-)analytical BEP models and the latter has not been used in the numerical modelling of BEP.

This equation is plotted in Fig. 10 as a function of the particle Reynolds number labelled as "Sellmeijer et al. (2011), d_{70} based". Because the calibration was performed assuming a d_{70} grain size, error margins of ±20% of the grain size are included in Fig. 10. It is assumed that $\frac{d_{70}}{d_{70,m}} = \frac{d_{50}}{d_{50,m}}$; therefore, the exponent of 0.6 in Eq. (22) remains the same.

Unlike shear stress-based type of onset of motion criteria, an example of a velocity-based criterion, as applied in BEP modelling (Zhou et al., 2012), is shown below.

$$u_{Hc} = K_c \sqrt{\frac{4gd_{50}f_f}{3(K_1 f_f + 1)C_x}\left(\frac{\rho_s}{\rho_w} - 1\right)} \tag{23}$$

$$u_{Vc} = \frac{\alpha}{K_v}\sqrt{\frac{4gd_{50}}{3C_d}\left(\frac{\rho_s}{\rho_w} - 1\right)} \tag{24}$$

In Eqs. (23) and (24) the grain-to-grain friction is expressed by the coefficient $f_f = 0.3$. $\alpha = 0.8$ is a coefficient that relates to the grain shape. $K_C = 1.5$, $C_d = 2.0$, $C_x = 1.0$, $K_v = 0.3$ and $K_1 = 0.3$ are unspecified coefficients. The pipe depth is assumed to be constant at 0.0015 m (Zhou et al., 2012). Eq. (23) is rewritten as a function of the Shields parameter using Eq. (19), the equation is plotted as a light blue line in Fig. 10. The figure shows that Eq. (23) is more conservative than most other approaches, because it assumes a lower critical value.

Fig. 10 shows the Shields diagram, where the y-axis represents the critical Shields parameter and on the x-axis the particle Reynolds number. The different onset of motion criteria used in numerical BEP models are displayed as lines. Crosses are used in case no model is given, but only a critical onset of motion value is provided. BEP experiments are displayed as grey dots and averages of experimental series as hollow circles or squares. This figure displays the wide range in onset of motion criteria that are applied in BEP modelling. This wide range will significantly impact the outcome of the BEP model. Additionally, the BEP experiments themselves show a large variability in critical Shields parameters although the range in grain sizes is limited. The regressions of BEP experiments by Pol et al. (2022) (displayed as grey patches) indicate that the critical Shields parameter becomes lower near the tip/larger near the exit. This may be attributed to a relatively large upward seepage through the pipe bottom close to the pipe tip (Pol et al., 2022). A similar trend was shown in the BEP centrifuge experiments by Okamura et al. (2022). Refining onset of motion criteria in BEP modelling is essential to ensure physically sound results. Models that are independent of the particle Reynolds number (White, 1940; Mantz, 1977; Briaud et al., 2017) do not capture dependence of the critical Shields parameter and the particle Reynolds number that is observed in BEP experiments. However, even models that do incorporate this dependency cannot accurately represent all BEP experiments. Therefore, more experimental research is required to refine the onset of motion criteria for secondary erosion.

When incorporating onset of motion criteria in groundwater flow models, the critical shear stress is often rewritten as a critical gradient $i_c = \frac{\delta h_c}{\delta x}$ in the x-direction parallel to the pipe bed, because this quantity can easily be derived from the groundwater flow calculations. For White's onset of motion criterion, this is done by combining Eqs. (18) and (21):

$$i_c = \frac{4\pi}{6}\frac{\rho'}{\rho_w}\frac{\eta d_x tan(\theta)}{Dh} \tag{25}$$

Assuming an infinitely wide pipe (parallel plates) ($Dh = 2a$) results in Eq. (26) (Sellmeijer, 2006).

$$i_c = \frac{\pi}{3}\frac{\rho'}{\rho_w}\frac{\eta d_x tan(\theta)}{a} \tag{26}$$

The shape of the pipe, the dimensions of the pipe and secondary erosion are strongly linked in the modelling of backward erosion piping. If the secondary erosion criterion is only applied at the bottom of the pipe, development of the pipe width is determined by a predefined cross-section shape. In BEP modelling this is often chosen as rectangular with a given width (w) over depth (a) ratio ($\frac{w}{a}$) (Van Beek et al., 2022; Robbins and Griffiths, 2021a) or circular (Rotunno et al., 2019). The assumption of the pipe shape can greatly impact the critical head; however, the true shape of the pipe is uncertain and difficult to predict. In lab experiments with rigid cover layers, very wide pipes are observed (Vandenboer et al., 2017), whereas in recent field experiments with natural clay covers, the pipe shapes were nearly circular at some locations. This difference between lab and field may be attributed to the presence of fines, the erodibility of the cover layer and the more gradual transition between aquitard and aquifer. As an alternative to predefining the shape of the pipe, it is possible to let the pipe develop freely within the domain, as happens in DEM modelling. Another approach is to average the gradients in the pipe and to assess secondary erosion in the entire pipe based on the average gradient (Aguilar-López et al., 2016).

The widening due to secondary erosion can be implemented in several ways in the numerical BEP model. If a fixed cross-section ratio is given, the deepening of the pipe results in a proportional widening of the pipe. When assuming a pipe of infinite width, the resulting pipe depth will be small because the cross-section is large. Esch et al. (2013) found pipe depths of approximately 30 grains in a large scale simulation. However, when assuming a round pipe, the resulting pipe depths will be significantly larger. Rotunno et al. (2019) found pipe depths of 100 grains or more in a large-scale simulation. The depth of the erosion channel increases with the scale of the experiment.

4.3. Sediment transport equations

To model time-dependent progression of the erosion channel, a transport equation is required in addition to time-dependent groundwater flow. These models often use a sediment mass conservation law, such as the Exner equation. In Eq. (27) a reformulated version is presented, with the pipe depth a [m] and the bedload transport q_b [m/s].

$$(1-n)\frac{\delta a}{\delta t} = \frac{\delta q_b}{\delta x} \tag{27}$$

The Exner equation states that the difference in incoming and outgoing sediment equals the bed level change in time.

The bedload transport is often expressed as a function of the dimensionless bedload transport q_b^*.

$$q_b = \frac{q_b^*}{(\rho_s - \rho_w) * g * \frac{d^3}{\nu}} \tag{28}$$

There are many different expressions for the dimensionless bedload transport. Table 3 provides an overview of the different transport equations that are used in BEP modelling.

The transport equations of Yalin, Charru, Cheng, and Ouriemi were used by Pol (2022) in comparison with BEP experiments and by Wewer et al. (2021) for the numerical modelling of BEP. Both studies showed that the transport equations by Yalin and Cheng perform best. A new calibration on flume experiments was performed by Pol et al. (2022). The resulting equation was further refined using BEP experiments. In the numerical model by Pol et al. (2024), onset of motion criteria for both primary and secondary erosion are used, but only a transport equation for secondary erosion is provided. The omission transport of the pipe tip is assumed to have a negligible effect. Another approach is to only use secondary erosion averaged over the entire pipe length. By relating the length of the pipe to the average depth, secondary erosion will also lead to lengthening of the pipe (Wewer et al., 2021). Computationally averaging the pipe depth over the pipe length is less expensive. However, there is no comparative study that assesses the impact of averaging the pipe depth. Consequently, the error made by this simplification is not quantified. The only model that incorporates transport equations for both primary and secondary erosion was developed by Rotunno et al. (2019). The model is calibrated based on several large-scale experiments but the calibrated values vary significantly between the different experiments (Callari and Pol, 2022); therefore, further validation is required. A model with a transport equation based on flow perpendicular to the pipe/aquifer interface was developed by Fujisawa (2016). The transport equation is based on heave experiments. However, this model does not seem to be validated by BEP experiments. Although (Rahimi et al., 2021) uses the term "time-dependent progression", the progression of the pipe is not based on a transport equation. Because of this, it is expected that the progression rate mainly depends on the imposed time step of the model (Pol, 2022). The model by Wang et al. (2014) uses a transport equation for sediment, but this is not coupled with transient groundwater flow and is therefore not a time-dependent model. DEM models are inherently time-dependent because their governing equations rely on Newton's second law of motion.

Since BEP is a time-dependent process, a single flood event might not result in immediate dike failure, as the pipe may not progress over the fully develop along the seepage path. Compared to the steady state assumption of the high water event assumed to be permanent, the estimated dike failure probability for a given design period is reduced by including time-dependence. The current time-dependent numerical models require additional validation and investigation; especially in large-scale 3D situations, the uncertainty of the existing models increases (Pol et al., 2024).

5. Discussion

Although the numerical modelling of BEP has improved significantly over the past decades, there are still numerous challenges and further improvements to be made. An overview of the most pressing challenges can be found in Table 4. These improvements are related to the following areas: the representation of BEP itself, the modelling of related processes such as uplift, heave, and macrostability, and the optimization of numerical methods.

5.1. Challenges in representing BEP

BEP is a process in which macro-scale groundwater flow interacts with micro-scale erosion processes. Modelling BEP is challenging due to this significant scale difference. One approach is to create a fundamental model using CFD-DEM, but this method is too computationally expensive to simulate BEP beneath a dike. Alternatively, a simplified model can be used, which relies on several assumptions to estimate micro-scale flow and erosion within the pipe, thus leading to a loss of accuracy. There are also approaches which do not simplify the flow in the pipe, but do simplify the erosion (Fujisawa, 2016). However, research in this type of modelling is limited. Additionally, hybrid modelling techniques such as those that combine continuum methods with DEM modelling could be a promising research direction.

Validation and calibration of all numerical models are limited, especially at larger scales. The number of available physical experiments is relatively small. When models require calibration of many parameters, the limited number of available experiments must be divided between calibration and validation. Most numerical modelling papers do not provide any validation or calibration based on experiments. The papers that do validate their models often only compare the critical hydraulic head, pipe length and pore pressures. Measurements of flow velocity,

Table 3
Transport equations used in numerical BEP modelling.

Equation	Ref.	Erosion type
$F = ma$	Newton	Both
$E = K_3 * (u_n - u_{cn})$	Wang et al. (2014)	Primary
$a = \frac{u_n}{n} - \left(f + (1-n)\frac{\delta p}{\delta X}\right)\frac{k}{n^2 \rho g}$	Fujisawa (2016)	Primary (heave)
$\dot{n} = c_n * (\tau_n - \tau_{cn})$	Rotunno et al. (2019)	Primary
$\dot{R} = \frac{c_r}{\rho_s} * (\tau - \tau_c)$	Rotunno et al. (2019)	Secondary
$q_b^* = 0.635 s\sqrt{\theta} * \left[1 - \frac{ln(1+a*s)}{a*s}\right]$	Yalin (1963)	Secondary (flume)
$q_b^* = 0.773 Re_p^{1.78} \theta^{3.12}$	Cheng (2004)	Secondary (flume)
$q_b^* = 0.025\theta(\theta - \theta_c)C_{vs}$	Charru et al. (2004)	Secondary (flume)
$q_b^* = \Phi \frac{\theta_c}{12}\left[\frac{\theta}{2*\theta_c} * (\frac{\theta^2}{\theta_c^2} + 1) - 0.2\right] C_{vs}$	Ouriemi et al. (2009)	Secondary (flume)
$q_b^* = 0.08 * \theta(\theta - \theta_c)$	Pol et al. (2024)	Secondary (flume), corrected for BEP progression rate

In Yalin: $a = 2.45\frac{\sqrt{\theta_c}}{\left(\frac{\rho_s}{\rho_w}\right)^{0.4}}$; $s = \frac{\theta - \theta_c}{\theta_c}$
Viscous scaling term: $C_{vs} = \frac{\sqrt{g*\rho_w(\rho_s - \rho_w)}d^{1.5}}{\eta_c}$

pipe depth, and pipe shape during physical experiments are limited to a few small-scale experiments. As a result, validation of micro-scale phenomena in BEP modelling is difficult as was pointed out by Pol et al. (2024). Validation of large-scale 3D set-ups poses additional challenges, as most large-scale experiments feature open outlets and allow multiple pipes to form, creating conditions that are nearly 2D (Van Beek et al., 2022). More experimental research incorporating micro-scale measurements is necessary to enhance the validation of numerical BEP models and improve their accuracy. Additionally, it is important that the numerical models are reproducible. Key requirements include availability of the input and output data as well as clear documentation of the workflow and on detailed documentation of model components (Zhu et al., 2023, 2025).

In BEP modelling, the flow inside the pipe requires further research. The pipe flow is either fully resolved or the flow is simplified. In the latter case either turbulent or laminar flow is assumed. The assumed flow regime also impacts the applicable secondary erosion criterion. However, there is no consensus, and flow regime assumptions vary across studies. Based on small-scale experiments laminar flow inside the pipe seems likely (Robbins and Van Beek, 2017). However, the flow regime is greatly dependent on the dimensions of the pipe, which increase with the scale of the water retaining structure. The flow regime in field-scale situations and the impact thereof on the BEP process are unknown. Similarly the pipe shape is often assumed to be smooth, whereas rough surfaces are more likely in BEP. The roughness and the representation thereof can greatly impact the resistance against the flow (Arfaie et al., 2018). The geometry of the pipe at the large scale, which greatly impacts (and is impacted by) the flow regime, is another uncertainty in BEP modelling. During a flood event, either one or multiple pipes are created, but it is difficult to estimate how many pipes are created and how heavily a single pipe is loaded. The amount of meandering, branching, and the cross-section variation of the pipe are not often included in BEP modelling. However, these factors do impact the flow velocity inside the pipe. Additionally, the flow is often assumed to be fully developed, which suggests that the velocity profile is constant over the entire length of the pipe, even though (especially near the tip) the flow is transitioning from the aquifer to the pipe. Similarly, the velocity profile and shear stresses at the pipe-aquifer interface are uncertain due to the unknown impact of upward seepage. The sediment in motion inside the pipe also has an impact on the flow and may cause an additional pressure loss. This process is observed in sandboils and may also significantly impact the headloss inside the pipe. Nevertheless, the impact of soil grains in suspension are generally not incorporated in BEP modelling.

Erosion is another great uncertainty. Erosion criteria and transport equations differ per author, but no universally accepted standard is available. Even the dominant type of erosion criterion for progression (primary or secondary erosion) differs per author. In the modelling of primary erosion, the models vary in both the equations that are used and the underlying philosophy. In order to better understand the erosion process, micro-scale measurements and calculations are required. Especially in heterogeneous situations, it is important to better understand the primary erosion mechanism. For instance, it is not clear when the pipe will begin to branch/braid or when the pipe will grow vertically underneath a barrier. Calibration of onset of motion criteria and transport equations, specifically of BEP experiments, is required to improve the basis of the numerical models. Fig. 10 demonstrates the wide variety in available onset of motion criteria used in BEP modelling. Nearly all models are based on flume experiments with tangential flow along the erosion surface. The BEP experiments by Pol et al. (2022) and Okamura et al. (2022) demonstrate that near the tip the critical shear stress is reduced. This might be explained by the upward seepage (more dominant near the tip) which reduces both the acting and critical shear stress (Cheng and Chiew, 1999; Francalanci et al., 2008; Lu et al., 2008). In the numerical model by Xiao et al. (2023), which assumes laminar pipe flow, this resulted in an increase of the hydraulic gradient near the tip of the pipe. A better understanding of upward seepage and the erosion at the interface is required. Transport equations are required for the time-dependent modelling of BEP, but as with the onset of motion criteria for secondary erosion, most models are based on flume experiments. The only BEP specific

Table 4
Key challenges in BEP modelling.

Challenge	Recommendations
The computational effort for DEM approaches to model the micro-scale process is too high for practical application, but the macro-scale modelling approaches (over-)simplify the problem	With time the computational capabilities are expected to increase. In the mean time hybrid modelling approaches (combining continuum and DEM modelling) may provide a solution.
The flow in the pipe is often simplified to laminar, 1-directional flow. However the impact of the flow regime, the of lateral influx and of grains in suspension on the shear stresses are relatively unknown, especially at larger scales	With numerical modelling using free fluid flow calculations inside of the pipe a better understanding of the flow in the pipe can be created. For a better understanding of influence of suspended sand grains on the flow velocity and shear stress, physical experiments are required.
Erosion criteria and transport equations in BEP modelling are mostly taken from flume experiments and open channel flow theory. However BEP experiments demonstrate significant differences due to the lateral influx.	A combination of experimental research and DEM modelling can be used to derive new erosion laws, for BEP, which include the lateral influx.
Because of a limited availability of experiments and the complexity of the problem, validation and bench-marking is difficult.	More micro-scale measurements of experiments at different scales are required to validate numerical models.

transport equation is defined by Pol (2022). Cea et al. (2024) used a method to combine different types of erosion and deposition processes. Deposition is not often included in BEP modelling, although it may lead to differences in the resulting pipe depth. Combining primary and secondary erosion with erosion due to lateral influxes and the deposition of sediments can be used to improve BEP modelling.

5.2. Related physical processes

Although this paper focuses on the numerical modelling of BEP, the approach for other physical processes can be beneficial to the prediction of BEP. Modelling BEP often does not consider the full failure path. In order for dike failure to occur due to backward erosion piping, the cover layer (if present) must be broken and heave of the sandy aquifer must occur. In the U.S. the assessment of BEP is mainly done through the evaluation of heave. However, in the numerical modelling of BEP it is not often incorporated. Many authors have modelled heave as a separate process (Martinez et al., 2017; Polanco-Boulware and Rice, 2016). In the prediction of BEP, numerical models would benefit from explicitly incorporating uplift and heave, especially since the resistance in the sand-boil can be significant (Robbins et al., 2020; Marchi et al., 2021).

The full failure of the dike due to BEP also includes the rapid widening of the pipe, loss of strength in the foundation, the lowering of the dike crest, the dike breach and finally flooding of the protected area. There is almost no experimental data available for the failure of dikes due to backward erosion piping; thus, model validation of the full failure process is difficult. Most models stop when the pipe has progressed to the upstream toe; however, breach modelling has been combined with piping by Chen et al. (2019). In these models a fully progressed pipe is used as the initial condition in the model, which widens and deepens until the roof collapses.

Similarly, it was suggested that the strength of the foundation decreases with the developing pipe; therefore, stability issues of the water retaining structure may already arise before the pipe has grown over the full seepage length (Rahimi et al., 2021). Coupling these types of mechanisms with BEP models could give engineers better estimates of the failure process. This would be less conservative than the current approach. More experimental research is required for the validation of the failure processes.

Backward erosion piping is one of four internal erosion mechanisms, along with contact erosion, concentrated leak erosion and suffusion (ICOLD, 2017). Suffusion and concentrated leak erosion are sometimes confused with BEP in literature, due to the use of terminology such as “piping”. However, it was recognized in Robbins (2022) and Pol (2022) that these mechanisms are not the same as BEP and should not be considered as such. Components of other types of internal erosion modelling, such as the increase of viscosity due to particles in suspension inside of the pipe (Fujisawa et al., 2010), might improve BEP modelling.

5.3. Computational methods

Current numerical methods for predicting BEP include DEM, LBM, FEM, FVM. However, these methods are either computationally too expensive, or use many assumptions and struggle in accurately representing microscale phenomena such as the flow at the pipe tip. Other numerical methods might help overcome this issue; methods that could be considered are: the extended finite element method XFEM; meshless methods such as smooth particle hydromechanics (SPH); Multigrid approaches and the material point method (MPM). An investigation into the application of these techniques in BEP modelling has not yet been conducted. SPH has been used to model internal erosion in the granular foundation of dikes, but the erosion equations used are more similar to suffusion than BEP (Ma et al., 2024). However, the research shows promise in using SPH to represent internal erosion and might become applicable to BEP.

Research on the numerical modelling of BEP mainly focuses on the representation of the physical process. Topics such as mesh convergence, stability and accuracy of the methods, choice of solvers, parallel computing, are not often discussed. The most elaborate studies on numerical aspects include the research by Robbins et al. (2022) and Robbins and Griffiths (2021a). These papers focus on the type of mesh element used to represent the pipe and the use of adaptive meshing to refine the mesh around the pipe tip respectively. Tran et al. (2017) and Froiio et al. (2019) applied parallelization and reported computational effort. Fascetti and Oskay (2019a) performed a mesh convergence study. Reporting and executing more of these types of numerical studies could lead to a broader understanding and eventually a more accurate representation of the flow in front of the pipe tip and reduced computational effort.

All models mentioned above aim to best predict BEP. However, it is also possible to use experimental data to back-calculate relevant parameters in FEM calculations. This inverse modelling technique is described and used by Bocovich (2019) and Peng and Rice (2020). This approach can be used to improve other numerical models, and to learn more about experiments. However, since it is essentially a calibration method, the results may have less physical meaning than desired.

To speed up calculations, numerical models may be replaced by machine learning algorithms. This method was first applied for BEP by Sellmeijer (2006) and has since been further applied in several internal erosion studies (Kaunda, 2015; Aguilar-López et al., 2016; Fascetti and Oskay, 2019a). The advantage of this approach is the relatively high speed at which a large number of calculations can be performed. The disadvantage is that it is trained (calibrated/validated) on a limited data set. Therefore, its application is only as good as the underlying data/simulations. A promising field of research for BEP modelling is physics informed machine learning algorithms; these algorithms integrate both physics and observational data (Cai et al., 2021).

6. Conclusion

In this paper, an overview of numerical BEP modelling is given. The assumptions and limitations of different approaches are discussed and several knowledge gaps are identified. These are defined as either the topics on which authors do not agree/use different approaches, or topics that are not mentioned and where there is no conclusive answer yet. Potential research directions to address these challenges are as follows:

- More large scale experiments with micro-scale measurements are required to improve the understanding of BEP and the validation of the numerical models
- Investigation into hybrid modelling approaches can reduce the number of simplifications required to model large-scale dikes, while not requiring the extreme computational effort of DEM modelling.
- More research is required on the flow in the pipe and the impact of assuming the flow to be linear, laminar, and not influenced by the meandering of the pipe.
- BEP specific erosion laws should be derived using a combination of experiments and DEM modelling.

In recent decades, numerical modelling of BEP has advanced significantly. It is now technically possible to perform 3D, time-dependent, numerical simulations using Darcyan flow combined with empirical erosion laws. However, there are still many improvements to be made and many topics for future research.

CRediT authorship contribution statement

E.M. van der Linde: Writing – original draft, Investigation, Conceptualization. **M. Wewer:** Writing – review & editing, Investigation, Conceptualization. **B.A. Robbins:** Writing – review & editing, Investigation. **O. Colomés:** Writing – review & editing, Supervision. **S.N. Jonkman:** Writing – review & editing, Supervision. **J.P. Aguilar-López:** Writing – review & editing, Supervision, Conceptualization.

Declaration of competing interest

The authors declare that they have no known competing financial interests or personal relationships that could have appeared to influence the work reported in this paper.

Data availability

Data will be made available on request.

References

Aguilar-López, J.P., Warmink, J.J., Schielen, R.M.J., Hulscher, S.J.M.H., 2016. Piping erosion safety assessment of flood defences founded over sewer pipes. European Journal of Environmental and Civil Engineering 22, 707–735. http://dx.doi.org/10.1080/19648189.2016.1217793.

Allan, R., 2018. Backward erosion piping. pp. 1–1012. http://dx.doi.org/10.1002/9781118577165.ch3.

Arfaie, A., Burns, A., Dorrell, R.M., Ingham, D.B., Eggenhuisen, J.T., McCaffrey, W.D., 2018. Optimisation of flow resistance and turbulent mixing over bed forms. Environmental Modelling & Software 107, 141–147.

Arrarás, A., Gaspar, F.J., Portero, L., Rodrigo, C., 2019. Mixed-dimensional geometric multigrid methods for single-phase flow in fractured porous media. SIAM Journal on Scientific Computing 41 (5), B1082–B1114.

Barendsen, L., 2020. The effect of leakage on backward erosion piping: A modelling study in 2D and 3D.

Bear, J., 1972. Dynamics of Fluids in Porous Media. Courier Corporation.

Bersan, S., Jommi, C., Koelewijn, A., Simonini, P., 2013. Applicability of the fracture flow interface to the analysis of piping in granular material. In: Proc., COMSOL Conference, Rotterdam, the Netherlands. pp. 23–25.

Bligh, W.G., 1910. Dams, barrages and weirs on porous foundations. Engineering news 64, 708–710.

Bocovich, C., 2019. Investigation of Backwards Erosion Piping by Data Driven Modeling. Colorado School of Mines.

Bonelli, S., 2013. In: Bonelli, S., Nicot, F. (Eds.), Erosion in geomechanics applied to dams and levees. John Wiley & Sons, Inc., Hoboken, NJ, USA, http://dx.doi.org/10.1002/9781118577165, URL: http://doi.wiley.com/10.1002/9781118577165.

Briaud, J.-L., Govindasamy, A.V., Shafii, I., 2017. Erosion charts for selected geomaterials. Journal of Geotechnical and Geoenvironmental Engineering 143 (10), 04017072.

Brinkgreve, R., Kumarswamy, S., Swolfs, W., Waterman, D., Chesaru, A., Bonnier, P., et al., 2016. PLAXIS 2016. PLAXIS bv, the Netherlands, pp. 1–16.

Brinkman, H.C., 1949. A calculation of the viscous force exerted by a flowing fluid on a dense swarm of particles. Flow, Turbulence and Combustion 1 (1), 27–34.

Cai, S., Mao, Z., Wang, Z., Yin, M., Karniadakis, G.E., 2021. Physics-informed neural networks (PINNs) for fluid mechanics: A review. Acta Mechanica Sinica 37 (12), 1727–1738.

Callari, C., Froiio, F., 2020. A hydromechanical finite element formulation for localized internal erosion in porous media, with application to backward piping in coffer-dams. International Journal for Multiscale Computational Engineering 18, 181–197. http://dx.doi.org/10.1615/IntJMultCompEng.2020031422.

Callari, C., Pol, J.C., 2022. Numerical interpretation of regressive localized internal erosion in a real-scale levee physical model. Geomechanics for Energy and the Environment 32, 100395.

Cao, Z., Pender, G., Meng, J., 2006. Explicit formulation of the Shields diagram for incipient motion of sediment. Journal of Hydraulic Engineering 132 (10), 1097–1099.

Carman, P.C., 1956. Flow of gases through porous media. No Title.

Cea, L., García-Feal, O., Nord, G., Piton, G., Legoût, C., 2024. Implementation of a GPU-enhanced multiclass soil erosion model based on the 2D shallow water equations in the software iber. Environmental Modelling & Software 179, 106098.

Charru, F., Mouilleron, H., Eiff, O., 2004. Erosion and deposition of particles on a bed sheared by a viscous flow. Journal of Fluid Mechanics 519, 55–80.

Chen, S.S., Zhong, Q.M., Shen, G.Z., 2019. Numerical modeling of earthen dam breach due to piping failure. Water Science and Engineering 12 (3), 169–178.

Cheng, N.-S., 2004. Analysis of bedload transport in laminar flows. Advances in water resources 27 (9), 937–942.

Cheng, N.-S., Chiew, Y.-M., 1999. Incipient sediment motion with upward seepage. Journal of Hydraulic Research 37 (5), 665–681.

COMSOL AB, 2024. Comsol multiphysics v. 5.4. reference manual. COMSOL Multiphysics software, www.comsol.com.

Danka, J., Zhang, L.M., 2015. Dike failure mechanisms and breaching parameters. Journal of Geotechnical and Geoenvironmental Engineering 141 (9), 04015039.

Di Felice, R., 1994. The voidage function for fluid-particle interaction systems. International journal of multiphase flow 20 (1), 153–159.

Ding, L., Wu, M., Liu, C., Sun, D., Yao, Q.L., 2007. Numerical simulation of dynamic development of piping in two-stratum dike foundations. Water Resources and Hydropower Engineering 38, 36–39.

Ergun, S., 1952. Fluid flow through packed columns. Chemical engineering progress 48, 89–94.

Esch, J.M.V., a. M. Teunissen, J., Stolle, D., 2013. Modeling transient groundwater flow under dikes and dams for stability assesment. p. 9.

Fang, Y., Guo, L., Hou, M., 2020. Arching effect analysis of granular media based on force chain visualization. Powder Technology 363, 621–628.

Fannin, R.J., Slangen, P., 2014. On the distinct phenomena of suffusion and suffosion. Géotechnique Letters 4, 289–294.

Fascetti, A., 2022. Data-and physics-based modeling of backward erosion piping. In: Civil Engineering for Disaster Risk Reduction. Springer, pp. 43–60.

Fascetti, A., Oskay, C., 2019a. Dual random lattice modeling of backward erosion piping. Computers and Geotechnics 105, 265–276. http://dx.doi.org/10.1016/j.compgeo.2018.08.018.

Fascetti, A., Oskay, C., 2019b. Multiscale modeling of backward erosion piping in flood protection system infrastructure. Computer-Aided Civil and Infrastructure Engineering 34 (12), 1071–1086.

Foster, M., Fell, R., Spannagle, M., 2000. The statistics of embankment dam failures and accidents. Canadian Geotechnical Journal 37, 1000–1024, URL: http://www.nrcresearchpress.com/doi/abs/10.1139/t00-030.

Francalanci, S., Parker, G., Solari, L., 2008. Effect of seepage-induced nonhydrostatic pressure distribution on bed-load transport and bed morphodynamics. Journal of Hydraulic Engineering 134 (4), 378–389.

Froiio, F., Callari, C., Rotunno, A.F., 2019. A numerical experiment of backward erosion piping: Kinematics and micromechanics. Meccanica 54, 2099–2117. http://dx.doi.org/10.1007/s11012-019-01071-7.

Fujisawa, K., 2016. Numerical analysis of backward erosion of soils by solving the Darcy–Brinkman equations. Advances in Computational Fluid-Structure Interaction and Flow Simulation: New Methods and Challenging Computations. Springer, pp. 193–201.

Fujisawa, K., Murakami, A., 2018. Numerical analysis of coupled flows in porous and fluid domains by the Darcy-Brinkman equations. Soils and Foundations 58 (5), 1240–1259.

Fujisawa, K., Murakami, A., Nishimura, S., 2010. Numerical analysis of the erosion and the transport of fine particles within soils leading to the piping phenomenon. Soils and Foundations 50, 471–482.

Geller, S., Krafczyk, M., Tölke, J., Turek, S., Hron, J., 2006. Benchmark computations based on lattice-Boltzmann, finite element and finite volume methods for laminar flows. Computers & fluids 35 (8–9), 888–897.

GEO-SLOPE International, 2015. Seepage Modeling with SEEP/W. GEO-SLOPE International.

Griffith, W., 1914. The stability of weir foundations on sand and soil subject to hydrostatic pressure. Minutes Proc. Inst. Civ. Eng. 197, 221–232.

Hanks, R.W., Ruo, H.C., 1966. Laminar-turbulent transition in ducts of rectangular cross section. Industrial & Engineering Chemistry Fundamentals 5 (4), 558–561.

Hanses, U., 1985. The mechanics of the development of erosion pipes in a layered substratum beneath dams. p. 214.

Hoffmans, G., Rijn, L.V., 2018. Hydraulic approach for predicting piping in dikes. Journal of Hydraulic Research 56, 268–281. http://dx.doi.org/10.1080/00221686.2017.1315747.

ICOLD, 2017. Bulletin 164 - internal erosion of existing dams, levees and dikes, and their foundations. Volume 1: Internal erosion processes and engineering assessment.

Itasca Consulting Group, I., 2023. FLAC3D — Fast Lagrangian analysis of continua in three-dimensions minneapolis: Itasca.

Jennings, A.A., Pisipati, R., 1999. The impact of Brinkman's extension of Darcy's law in the neighborhood of a circular preferential flow pathway. Environmental Modelling & Software 14 (5), 427–435.

Joseph, D.D., Nield, D.A., Papanicolaou, G., 1982. Nonlinear equation governing flow in a saturated porous medium. Water Resources Research 18 (4), 1049–1052.

Kandhai, D., Vidal, D.J.E., Hoekstra, A., Hoefsloot, H., Iedema, P., Sloot, P.M.A., 1998. A comparison between lattice-Boltzmann and finite-element simulations of fluid flow in static mixer reactors. International Journal of Modern Physics C 9 (08), 1123–1128.

Kanning, W., Calle, E.O.F., 2013. Derivation of a representative piping resistance parameter based on random field modelling of erosion paths. Georisk 7, 99–109. http://dx.doi.org/10.1080/17499518.2013.790735.

Kaunda, R.B., 2015. A neural network assessment tool for estimating the potential for backward erosion in internal erosion studies. Computers and Geotechnics 69, 1–6. http://dx.doi.org/10.1016/j.compgeo.2015.04.010.

Lane, E.W., 1935. Security from under-seepage masonry dams on earth foundations. Transactions of the American Society of Civil Engineers 100, 1235–1272.
Li, H., Li, J., Yuan, H., 2018. A review of the extended finite element method on macrocrack and microcrack growth simulations. Theoretical and Applied Fracture Mechanics 97, 236–249.
Liang, Y., Yeh, T.-C.J., Wang, Y., Liu, M., Wang, J., Hao, Y., 2017. Numerical simulation of backward erosion piping in heterogeneous fields. Water Resources Research 53, 3246–3261. http://dx.doi.org/10.1002/2013WR014979.Reply.
Lominé, F., Scholtès, L., Sibille, L., Poullain, P., 2013. Modeling of fluid – solid interaction in granular media with coupled lattice Boltzmann discrete element methods : Application to piping erosion. International Journal for Numerical and Analytical Methods in Geomechanics 37, 577–596. http://dx.doi.org/10.1002/nag.
Lu, Y., Chiew, Y.-M., Cheng, N.-S., 2008. Review of seepage effects on turbulent open-channel flow and sediment entrainment. Journal of Hydraulic Research 46 (4), 476–488.
Ma, G., Bui, H.H., Lian, Y., Nguyen, T.V., Nguyen, G.D., 2024. Prediction of backward erosion, pipe formation and induced failure using a multi-physics SPH computational framework. International Journal for Numerical and Analytical Methods in Geomechanics.
Mantz, P.A., 1977. Incipient transport of fine grains and flakes by fluids—extended Shields diagram. Journal of Hydraulic Engineering 103 (6), 601–615.
Marchi, M., Martínez, M.F.G., Gottardi, G., Tonni, L., 2021. Field measurements on a large natural sand boil along the river Po, Italy. Quarterly Journal of Engineering Geology & Hydrogeology 54 (4), qjegh2020–097.
Martinez, M.F.G., Marchi, M., Tonni, L., Gottardi, G., Bezuijen, A., Rosso, A., 2017. Numerical simulation of the groundwater flow leading to sand boil reactivation in the Po River.
Moody, L.F., 1944. Friction factors for pipe flow. Transactions of the American Society of mechanical engineers 66 (8), 671–678.
Navin, M.P., Shewbridge, S., 2017. Example of 2D finite element analyses to inform backward erosion piping evaluation of a typical levee cross-section. pp. 32–45. http://dx.doi.org/10.1061/9780784480717.004.
Nguyen, V.P., Rabczuk, T., Bordas, S., Duflot, M., 2008. Meshless methods: A review and computer implementation aspects. Mathematics and computers in simulation 79 (3), 763–813.
Ni, X., Wang, Y., Chen, K., Zhao, S., 2015. Improved similarity criterion for seepage erosion using mesoscopic coupled PFC–CFD model. Journal of Central South University 22, 3069–3078. http://dx.doi.org/10.1007/s11771-015-2843-9, URL: http://link.springer.com/10.1007/s11771-015-2843-9.
Nie, Y.-p., Sun, D.-y., Wang, X.-k., 2022. Quantitative analysis of the erosion process in horizontal cobble and gravel embankment piping via CFD-DEM coupling method. Journal of the Brazilian Society of Mechanical Sciences and Engineering 44 (12), 1–16.
Nield, D.A., 1991. The limitations of the Brinkman-Forchheimer equation in modeling flow in a saturated porous medium and at an interface. International Journal of Heat and Fluid Flow 12 (3), 269–272.
Ojha, C.S.P., Singh, V.P., Adrian, D.D., 2003. Determination of critical head in soil piping. Journal of Hydraulic Engineering 129, 511. http://dx.doi.org/10.1061/(ASCE)0733-9429(2003)129:7(511), URL: http://link.aip.org/link/JHEND8/v129/i7/p511/s1&Agg=doi.
Okamura, M., Kusube, N., 2025. Prediction of hydraulic gradient for backward erosion piping in river levees considering flow regime and pipe geometry. Soils and Foundations 65 (2), 101591.
Okamura, M., Tsuyuguchi, Y., Izumi, N., Maeda, K., 2022. Centrifuge modeling of scale effect on hydraulic gradient of backward erosion piping in uniform aquifer under river levees. Soils and Foundations 62 (5), 101214.
Ouriemi, M., Aussillous, P., Guazzelli, E., 2009. Sediment dynamics. Part 1. Bed-load transport by laminar shearing flows. Journal of Fluid Mechanics 636, 295–319.
Ouyang, L.-B., Arbabi, S., Aziz, K., 1998. A single-phase wellbore-flow model for horizontal, vertical, and slanted wells. Spe Journal 3 (02), 124–133.
Peng, S., Rice, J.D., 2020. Inverse analysis of laboratory data and observations for evaluation of backward erosion piping process. Journal of Rock Mechanics and Geotechnical Engineering 12 (5), 1080–1092.
Perumal, D.A., Dass, A.K., 2015. A review on the development of lattice Boltzmann computation of macro fluid flows and heat transfer. Alexandria Engineering Journal 54 (4), 955–971.
Pol, J.C., 2020. Shields-Darcy pipingmodel. Verschilanalyse met Sellmeijer en D-GeoFlow.
Pol, J., 2022. Ph.D. thesis Piping to be published (Ph.D. thesis). Delft University of Technology, To be published.
Pol, J.C., Kanning, W., Van Beek, V.M., Robbins, B.A., Jonkman, S.N., 2022. Temporal evolution of backward erosion piping in small-scale experiments. Acta Geotechnica 1–22.
Pol, J.C., Noordam, A., Kanning, W., 2024. A 3D time-dependent backward erosion piping model. Computers and Geotechnics 167, 106068.
Polanco-Boulware, L., Rice, J.D., 2016. Reliability-based three-dimensional assessment of internal erosion potential due to crevasse splays. Journal of Geotechnical and Geoenvironmental Engineering 143, 1–12. http://dx.doi.org/10.1061/(ASCE)GT.1943-5606.0001596, URL: http://ascelibrary.org/doi/10.1061/%28ASCE%29GT.1943-5606.0001596.
Pritchard, P.J., Mitchell, J.W., 2016. Fox and Mcdonald's Introduction to Fluid Mechanics. John Wiley & Sons.
Rahimi, M., Shafieezadeh, A., 2020. Coupled backward erosion piping and slope instability performance model for levees. Transportation Geotechnics 24, http://dx.doi.org/10.1016/j.trgeo.2020.100394.
Rahimi, M., Shafieezadeh, A., Wood, D., Kubatko, E.J., 2021. A physics-based approach for predicting time-dependent progression length of backward erosion piping. Canadian Geotechnical Journal 58, 995–1004. http://dx.doi.org/10.1139/cgj-2019-0854.
Rice, J., Van Beek, V., Bezuijen, A., 2021. History and future of backward erosion research. ASCE, Washington, D.C., pp. 1–23.
Robbins, B.A., 2016. Numerical Modeling of Backward Erosion Piping. Itasca Consulting Group, Lima, Peru, pp. 551–558.
Robbins, B.A., 2022. Finite Element Modeling of Backward Erosion Piping (Ph.D. thesis). Colorado School of Mines.
Robbins, B.A., van Beek, V.M., Pol, J.C., Griffiths, D.V., 2022. Errors in finite element analysis of backward erosion piping. Geomechanics for Energy and the Environment 100331.
Robbins, B.A., Griffiths, D.V., 2018a. Internal Erosion of Embankments: A Review and Appraisal. American Society of Civil Engineers, Denver, CO, pp. 1–16.
Robbins, B.A., Griffiths, D.V., 2018b. In: Bonelli, S., Jommi, C., Sterpi, D. (Eds.), Modelling of Backward Erosion Piping in Two- and Three- Dimensional Domains. Vol. 17, Springer Nature Switzerland AG, Cham, Switzerland, pp. 149–158. http://dx.doi.org/10.1007/978-3-319-99423-9.
Robbins, B.A., Griffiths, D.V., 2021a. A two-dimensional, adaptive finite element approach for simulation of backward erosion piping. Computers and Geotechnics 129, 103820. http://dx.doi.org/10.1016/j.compgeo.2020.103820.
Robbins, B.A., Griffiths, D.V., 2021b. Quantifying the performance of piping mitigation measures with two-dimensional, adaptive finite element analysis. In: Proceedings of the 20th International Conference on Soil Mechanics and Geotechnical Engineering, Sydney.
Robbins, B.A., Griffiths, D.V., 2022. Analysis of backward erosion piping by critical secant gradient functions. pp. 555–560.
Robbins, B.A., Griffiths, D.V., Fenton, G.A., 2021. Random finite element analysis of backward erosion piping. Computers and Geotechnics 138, 1–14.
Robbins, B.A., Montalvo-Bartolomei, A.M., Griffiths, D.V., 2020. Analyses of backward erosion progression rates from small-scale flume experiments. Journal of Geotechnical and Geoenvironmental Engineering 146, 04020093. http://dx.doi.org/10.1061/(asce)gt.1943-5606.0002338, URL: https://orcid.org.
Robbins, B.A., Van Beek, V.M., 2017. Physical measurements of the backward erosion piping. pp. 29–37.
Romeo, E., Royo, C., Monzón, A., 2002. Improved explicit equations for estimation of the friction factor in rough and smooth pipes. Chemical engineering journal 86 (3), 369–374.
Rosenbrand, E., Van Beek, V.M., 2021. Numerical simulation of a large-scale backward erosion piping experiment in 2D and in 3D. In: 10th International Conference on Scour and Erosion. ASCE, Washington, D.C., pp. 70–82.
Rotunno, A.F., Callari, C., Froiio, F., 2017. In: Fremond, M., Maceri, F., Vairo, G. (Eds.), Computational Modeling of Backward Erosion Piping. Vol. 8, Springer, pp. 225–234. http://dx.doi.org/10.1007/978-3-319-48884-4, URL: http://link.springer.com/10.1007/978-3-319-48884-4.
Rotunno, A.F., Callari, C., Froiio, F., 2019. A finite element method for localized erosion in porous media with applications to backward piping in levees. International Journal for Numerical and Analytical Methods in Geomechanics 43, 293–316. http://dx.doi.org/10.1002/nag.2864.
Saliba, F., Nassar, R.B., Khoury, N., Maalouf, Y., Nassar, R.B., Khoury, N., Maalouf, Y., 2019. Internal Erosion and Piping Evolution in Earth Dams Using an Iterative Approach. ASCE, Philadelphia, PA, pp. 67–75.
Schlauch, E., Ernst, M., Seto, R., Briesen, H., Sommerfeld, M., Behr, M., 2013. Comparison of three simulation methods for colloidal aggregates in Stokes flow: Finite elements, lattice Boltzmann and Stokesian dynamics. Computers & fluids 86, 199–209.
Schmertmann, J.H., 2000. The no-filter factor of safety against piping through sands. In: Judgment and Innovation: The Heritage and Future of the Geotechnical Engineering Profession. ASCE, pp. 65–132.
Sellmeijer, J.B., 1988. On the mechanism of piping under impervious structures. p. 116.
Sellmeijer, J., 2006. Numerical computation of seepage erosion below dams (piping).
Sellmeijer, J.B., Calle, E.O.F., Sip, J.W., 1989. Influence of aquifer thickness on piping below dikes and dams. International Commision on Large Dams, Copenhagen, Denmark, pp. 357–366.
Sellmeijer, J.B., de la Cruz, J.L., Van Beek, V.M., Knoeff, H., 2011. Fine-tuning of the backward erosion piping model through small-scale , medium-scale and IJkdijk experiments. European Journal of Environmental and Civil Engineering 15, 1139–1154. http://dx.doi.org/10.3166/EJECE.15.1139-1154.
Sellmeijer, J.B., Koenders, M.A., 1991. A mathematical model for piping. Applied Mathematical Modelling 15, 646–651. http://dx.doi.org/10.1016/S0307-904X(09)81011-1, URL: http://linkinghub.elsevier.com/retrieve/pii/S0307904X09810111.

Shamy, U.E., Aydin, F., 2008. Multiscale modeling of flood-induced piping in river levees. Journal of Geotechnical and Geoenvironmental Engineering 1385–1398, URL: http://link.aip.org/link/?JGGEFK/134/1385/1.

Sibille, L., Lominé, F., Poullain, P., Sail, Y., Marot, D., 2015. Internal erosion in granular media: direct numerical simulations and energy interpretation. Hydrological Processes 29, 2149–2163. http://dx.doi.org/10.1002/hyp.10351, URL: http://doi.wiley.com/10.1002/hyp.10351.

Silvis, F., 1991. Verificatie Piping Model: Proeven in de Deltagoot. Waterloopkundig Laboratorium, Delft, The Netherlands.

Smith, M., 2009. ABAQUS/Standard user's manual.

Smith, I.M., Griffiths, D.V., 2004. Programming the finite element method. URL: https://books.google.nl/books?id=9ry7C2Hiv9QC.

Spiga, M., Morino, G.L., 1994. A symmetric solution for velocity profile in laminar flow through rectangular ducts. International communications in heat and mass transfer 21 (4), 469–475.

Taylor, R.L., 2014. FEAP-A finite element analysis program.

Tosun, I., Uner, D., Ozgen, C., 1988. Critical Reynolds number for Newtonian flow in rectangular ducts. Industrial & engineering chemistry research 27 (10), 1955–1957.

Tran, D.K., Prime, N., Froiio, F., Callari, C., Vincens, E., 2017. Numerical modelling of backward front propagation in piping erosion by DEM-LBM coupling. European Journal of Environmental and Civil Engineering 21, 960–987. http://dx.doi.org/10.1080/19648189.2016.1248794.

Van Beek, V.M., 2015. Backward Erosion Piping: Initiation and Progression. Technische Universiteit Delft, pp. 1–286. http://dx.doi.org/10.1007/s13398-014-0173-7.2.

Van Beek, V.M., Bezuijen, A., Sellmeijer, J.B., Barends, F., 2014. Initiation of backward erosion piping in uniform sands. Geotechnique 64 (12), 927–941.

Van Beek, V.M., Knoeff, H., Schweckendiek, T., 2011. Piping: Over 100 years of experience.

Van Beek, V.M., Robbins, B.A., Hoffmans, G., Bezuijen, A., van Rijn, L., 2019. Use of incipient motion data for backward erosion piping models. International Journal of Sediment Research 34, 401–408. http://dx.doi.org/10.1016/j.ijsrc.2019.03.001.

Van Beek, V., Robbins, B., Rosenbrand, E., van Esch, J., 2022. 3D modelling of backward erosion piping experiments. Geomechanics for Energy and the Environment 100375.

Van der Meij, R., 2024. D-Geo Flow User Manual. Deltares.

Van Rijn, L.C., 1984. Sediment transport, part I: Bed load transport. Journal of Hydraulic Engineering 110 (10), 1431–1456.

Vandenboer, K., 2019. A study on the mechanisms of backward erosion piping.

Vandenboer, K., Van Beek, V.M., Bezuijen, A., 2014. 3D finite element method (FEM) simulation of groundwater flow during backward erosion piping. Frontiers of Structural and Civil Engineering 8, 160–166. http://dx.doi.org/10.1007/s11709-014-0257-7, URL: http://link.springer.com/10.1007/s11709-014-0257-7.

Vandenboer, K., Van Beek, V.M., Bezuijen, A., 2017. Pipe depth measurement in small-scale backward erosion piping experiments. pp. 21–28.

Vandenboer, K., Van Beek, V.M., Bezuijen, A., 2019. Analysis of the pipe depth development in small-scale backward erosion piping experiments. Acta Geotechnica 14, 477–486. http://dx.doi.org/10.1007/s11440-018-0667-0.

Vermeulen, P.T.M., 2013. iMOD version 2.7 - interactive modeling, manual, deltares.

Wang, D., Fu, X., Jie, Y., Dong, W., Hu, D., 2014. Simulation of pipe progression in a levee foundation with coupled seepage and pipe flow domains. Soils and Foundations 54, 974–984. http://dx.doi.org/10.1016/j.sandf.2014.09.003.

Wang, Y., Ni, X., 2013. Hydro-mechanical analysis of piping erosion based on similarity criterion at micro-level by PFC 3D. European Journal of Environmental and Civil Engineering 17, s187–s204. http://dx.doi.org/10.1080/19648189.2013.834594, URL: http://www.tandfonline.com/doi/abs/10.1080/19648189.2013.834594.

Wewer, M., Aguilar-López, J.P., Kok, M., Bogaard, T., 2021. A transient backward erosion piping model based on laminar flow transport equations. Computers and Geotechnics 132, http://dx.doi.org/10.1016/j.compgeo.2020.103992.

White, C.M., 1940. The equilibrium of grains on the bed of a stream. Proceedings of the Royal Society of London. Series A. Mathematical and Physical Sciences 174, 322–338. http://dx.doi.org/10.1098/rspa.1940.0023, URL: http://rspa.royalsocietypublishing.org/cgi/doi/10.1098/rspa.1940.0023.

Xiao, Y., Cao, H., Luo, G., 2019. Experimental investigation of the backward erosion mechanism near the pipe tip. Acta Geotechnica 14, 767–781. http://dx.doi.org/10.1007/s11440-019-00779-w.

Xiao, Y., Pan, H., Luo, G., 2023. Modelling of flow in backward erosion pipes. Geomechanics for Energy and the Environment 100476.

Yalin, M.S., 1963. An expression for bed-load transportation. Journal of Hydraulic Engineering 89 (3), 221–250.

Zhang, X., Wang, C.-Y., Wong, H., Jiang, T., Dong, J., 2022. Modeling dam deformation in the early stage of internal seepage erosion–application to the teton dam, idaho, before the 1976 incident. Journal of Hydrology 605, 127378.

Zhou, X., Jie, Y., Li, G., 2012. Numerical simulation of the developing course of piping. Computers and Geotechnics 44, 104–108. http://dx.doi.org/10.1016/j.compgeo.2012.03.010, URL: http://linkinghub.elsevier.com/retrieve/pii/S0266352X12000511.

Zhu, Z., Chen, M., Qian, Z., Li, H., Wu, K., Ma, Z., Wen, Y., Yue, S., Lü, G., 2023. Documentation strategy for facilitating the reproducibility of geo-simulation experiments. Environmental Modelling & Software 163, 105687.

Zhu, Z., Chen, M., Ren, G., He, Y., Sun, L., Zhang, F., Wen, Y., Yue, S., Lü, G., 2025. A framework for assessing the computational reproducibility of geo-simulation experiments. Environmental Modelling & Software 106323.